AD A089141

JASON

12

LEVEL II

Technical Report

JSR-79-11

April 1980

TUNNEL DETECTION

By. J. F. Vesecky
W. A. Nierenberg
A. M. Despain

DTIC
ELECTE
SEP 9 1980
D
C

This document has been approved for public release and sale; its distribution is unlimited.

SRI International
1611 North Kent Street
Arlington, Va 22209

FILE COPY

80 9 5 040

SRI International

JASON

Technical Report

JSR-79-11

April 1980

TUNNEL DETECTION

By: J. F. Vesecky
W. A. Nierenberg
A. M. Despain

DTIC
ELECTE
SEP 9 1980
D
C

SRI International
1611 North Kent Street
Arlington, Virginia 22209

This document has been approved for public release and sale; its distribution is unlimited.

UNCLASSIFIED

SECURITY CLASSIFICATION OF THIS PAGE (When Data Entered)

REPORT DOCUMENTATION PAGE

READ INSTRUCTIONS BEFORE COMPLETING FORM

1. REPORT NUMBER: JSR-79-11

2. GOVT ACCESSION NO.: AD-A089141

3. RECIPIENT'S CATALOG NUMBER:

4. TITLE (and Subtitle): (6) Tunnel Detection,

5. TYPE OF REPORT & PERIOD COVERED: (4) Technical Report

6. PERFORMING ORG. REPORT NUMBER: (14) SRI-JSR-79-11

7. AUTHOR(s): (10) J. F. Vesecky, W. A. Nierenberg, A. M. Despain

8. CONTRACT OR GRANT NUMBER(s): (15) MDA903-78-C-0086, ARPA Order-2504

9. PERFORMING ORGANIZATION NAME AND ADDRESS:
SRI International
1611 North Kent Street
Arlington, VA 22209

10. PROGRAM ELEMENT, PROJECT, TASK AREA & WORK UNIT NUMBERS:
A.O. 2504,27,28

11. CONTROLLING OFFICE NAME AND ADDRESS:
Defense Advance Research Projects Agency
1400 Wilson Boulevard
Arlington, VA 22209

12. REPORT DATE: (11) Apr[illegible]80

13. NO. OF PAGES: 102 (12) 144

14. MONITORING AGENCY NAME & ADDRESS (if diff. from Controlling Office):

15. SECURITY CLASS. (of this report): Unclassified

15a. DECLASSIFICATION/DOWNGRADING SCHEDULE: NA

16. DISTRIBUTION STATEMENT (of this report)

Cleared for open publication, distribution unlimited.

17. DISTRIBUTION STATEMENT (disclaimer) The views and conclusions contained in this document are those of the authors and should not be interpreted as necessarily representing the official policies, either expressed or implied, of the Advance Research Projects Agency or the U.S. Government.

18. SUPPLEMENTARY NOTES

19. KEY WORDS (Continue on reverse side if necessary and identify by block number)

Tunnels
Tunnel Detection
Bore holes

20. ABSTRACT (Continue on reverse side if necessary and identify by block number)

This report investigates the problem of detecting tunnels; it focuses on the characteristics of the propagating medium and on techniques using compressional seismic (P) and electromagnetic (EM) waves propagating between sources and sensors located in boreholes at depths comparable with the tunnel for which one is searching. The interaction of P and EM waves with tunnels and with the surrounding media is studied as are detection methods in a general sense. This work has not looked into the specifics of sources, sensors and ambient noise levels.

DD FORM 1 JAN 73 1473

EDITION OF 1 NOV 65 IS OBSOLETE

UNCLASSIFIED

SECURITY CLASSIFICATION OF THIS PAGE (When Data Entered)

384941

TL

19. KEY WORDS (Continued)

20 ABSTRACT (Continued)

Accession For
NTIS GRA&I
DDC TAB
Unannounced
Justification
By
Distribution/
Availability Codes
Dist | Avail and/or special

CONTENTS

LIST OF FIGURES

LIST OF TABLES

I. INTRODUCTION, SUMMARY AND CONCLUSIONS

The discovery in late 1974 and early 1975 of North Korean tunnels beneath the Korean Demilitarized Zone focused attention on tunneling as a means of clandestinely placing intelligence agents and possibly larger forces a kilometer or more inside South Korean territory. In October, 1978, a third tunnel was discovered which, if completed, could have infiltrated about one division of fully armed troops per hour into South Korea. The United Nations Command responded by deploying various existing tunnel detection techniques as quickly as possible. On a longer time scale the Defense Advanced Research Projects Agency (DARPA) originated a program to explore new tunnel detection techniques applicable not only to the Korean problem, but also to tunnel detection in general. This report describes investigations in support of this DARPA research program.

While the motivation for this research arose from the desire to detect clandestine military tunneling, applications also exist in the discovery and exploration of non-military tunnels and other underground features resembling tunnels. For example, many unlocated mining tunnels exist from century old workings in what are now populated areas, e.g., in the county of Derbyshire, England. Surveys of such tunnels are necessary to insure the stability of surface structures above them.

A. North Korean Tunnels Beneath the Korean Demilitarized Zone

Since three North Korean tunnels have already been discovered (Korean Overseas Information Service, 1975, & Hoon, 1978) it is useful to describe briefly how these discoveries took place and outline the characteristics of the tunnels discovered.

1. Tunnel Discoveries

The first tunnel came to light in November of 1974 when a Republic of Korea (ROK) Army patrol noted significant variation in the vegetation pattern along a linear path and later steam escaping from the ground. Subsequent investigation revealed a very shallow tunnel--only a few feet below the surface. A warm North Korean lunchbox and various personal effects attested to the fact that tunnel construction was still underway at the time of discovery. This tunnel, known as the "Chang Jong-Ni Tunnel," is located near Korangpo in the western sector of the Demilitarized Zone (DMZ).

The second tunnel is located at Sobang-San near P'Yonggang in the central DMZ. It had been a suspected tunneling site since November, 1973, when a large number of explosions were monitored and troops in the DMZ felt ground tremors. This information plus photographic and defector intelligence gave a general idea of the tunnel location. Subsequent seismic listening activities enabled ROK scientists and geologists to locate the tunnel more exactly by means of triangulation. It is not clear from present information precisely what techniques were used but apparently the relative intensities of blasting and drilling noises

observed at a number of locations played a key role. It should be noted at this point that several thousand explosions occur each month near the DMZ from such sources as fortification construct , artillery practice, and even civilian mining operations.

Based upon this more refined location, a drilling campaign was instituted in which sixty-nine 7.5cm boreholes, each 100m deep, were to be drilled along a 225m strip transverse to the suspected tunnel path. Upon discovery in December, 1974, 44 of the 69 holes had been completed. At thousands of dollars per hole, the drilling operation represents considerable expense. The borehole which did in fact break into the tunnel was most strikingly noted by the loss of some 6000 liters of drilling fluid after the breakthrough. Examination of core samples, borehole photography and finally an intercept tunnel confirmed the discovery.

The third tunnel, discovered in October, 1978, passes under the demilitarized zone (DMZ) at a location about 40 km northwest of Seoul. This unfinished tunnel extends some 425 meters into South Korea about 1.7km southwest of Camp Kittyhawk, a U.S. advance post supporting the U.N. forces in the DMZ. An underground explosion, apparently caused by the North Korean tunnelers, led to the discovery of the tunnel. Nevertheless, three months of digging and drilling by South Korean engineers was required to locate the tunnel precisely and dig a counter tunnel to a depth of 70 meters.

2. Characteristics of the Discovered Tunnels

The tunnels fall into two classes, shallow and deep. The Chong Jong-Ni tunnel was very shallow, averaging only about 0.5m below the surface. Being in soil, the tunnel was lined along the sides and roof with reinforced concrete slabs. The cross section was approximately square, 1.2m on a side. The tunnel was about 4km long, extending some 1.2km south of the military demarcation line. Waste was removed by a narrow gage rail line and mining carts. Ventilation was by means of vents to the surface at intervals along the tunnel. No mention is made in the available reports of electric power lines for lighting or other uses. Most of the tunnel was destroyed by explosives, but a section was retained for historical interest and sensor experimentation.

The Sobang-San tunnel is considerably more elaborate, being blasted and drilled through granite some 50 to 100m below the surface. No roof support was evident in photographs of the tunnel interior. Its cross section is approximately rectangular with a flat floor, 2.2m wide, slightly concave walls and a 2m high arched roof. The walls and roof are rather rough and typical of mining tunnels. The total length is about 3.5km with several turns and sloping sections penetrating about 2km south of the military demarcation line. Ventilation was by mechanical blower and ducts. Electrical lines for lighting and power were run along the tunnel and waste removal was by mining carts along a narrow gage railway. A good deal of the southern end of the tunnel was backfilled by the North Koreans and subsequently cleared by the United Nations Command after the intercept tunnel was completed. Both sides have now fortified sections of the tunnel and peer at each other across the demarcation line.

The recently discovered tunnel near Camp Kittyhawk is similar to the Sobang-San tunnel. It was dug at depths of around 60m through granite with a diameter of some 2-3m. The tunnel extends some 435m into South Korea, having crossed the demilitarized zone. Such a tunnel, if completed, could infiltrate about one division of fully armed troops per hour into South Korea.

B. Summary of JASON Summer Study Investigations

Tunnel detection has much in common with exploration geophysics and naturally draws on many of the same techniques including seismic waves, electromagnetic waves, ground resistivity and many others. A good introduction to a wide variety of geophysical exploration methods is given by Telford, et al, (1976) while methods directed specifically at tunnel detection are reviewed by Systems Planning Corporation (1979). The JASON Summer Study effort has focused on the characteristics of the propagating medium and on techniques using compressional seismic (P) and electromagnetic (EM) waves propagating between sources and sensors located in boreholes at depths comparable with the tunnel for which one is searching. Borehole sensors are advantageous because wave propagation paths are shorter and because near-surface layers usually scatter and attenuate waves more strongly than do deeper layers. Our investigations deal with the interaction of P and EM waves with tunnels and with the surrounding media and on detection methods in a general sense. We have not looked into the specifics of sources, sensors and ambient noise levels except to note the existence of appropriate sources and sensors and the approximate amounts of signal loss that can be tolerated in a realistic

system. While these factors are clearly important they are beyond the scope of the present study.

In Chapter II we examine the P and EM wave propagation characteristics of subterranean media in general and consider the case of weathered granite, typical of the DMZ, in more detail. In comparing P and EM waves we have taken as comparable, waves having the same wavelength in the medium. For example, a wavelength of 6.3m resonates with a 1m radius tunnel. In monolithic granite EM waves at 28 MHz and P waves at 720 Hz have about this wavelength. For comparable wavelengths of ~ 3m P waves suffer only about one-tenth the power attenuation rate (0.13 dB m^{-1}) of EM waves (2.2 dB m^{-1}). The EM wave power attenuation rate grows more slowly with frequency (approximately as $\sqrt{f}$) in the 10-100 MHz range than does the P wave attenuation rate (approximately as f) over the comparable frequency range. In underground exploration, inhomogeneities in the medium can, through scattering, affect tunnel detection systems as much as or more than the large propagation loss. Inhomogeneities can mimic tunnels, causing false alarms in the detection system as well as providing unwanted "clutter" signal paths between source and sensor. The natural weathering process of granite rock causes joints (cracks) along fairly well-defined and approximately parallel planes. These joints of varying width fill with clay minerals as weathering progresses. Modeling the granite-clay-granite sandwich as simple slabs, we find power reflection coefficients as high as 0.3 for EM waves incident on weathered joints having widths in excess of about 20cm. For P waves incident on weathered joints having widths of a few centimeters and more, power reflection coefficients reach 0.9. Since

many weathered joints are likely to exist between source and sensor (depending on geological setting), scattering in the medium and hence false alarm and clutter signals could be a serious problem. Any detection system for general use will have to deal with this problem.

In Chapter III we consider a particular tunnel detection system, forward scatter between borehole sources and sensors, in some detail. The data collection scheme involves two or more boreholes, each having one or more sources or sensors. Detection is accomplished by transmitting EM or P waves from one borehole to another and noting the effect of the tunnel (if there is one) on the spatial distribution of received intensity and phase along the sensor borehole. First we discuss forward scatter by a cylindrical object, noting that the rock-air interface at the tunnel wall reflects normally incident P waves very efficiently for a wide variety of rock types. For EM waves at normal incidence the rock-air interface has power reflection coefficients varying from about 0.5 to 0.8 for a wide variety of rock types. After discussing a number of possible schemes to model scattering from a cylindrical tunnel, we consider a very simple model in some detail. Here we model the tunnel as a thin, opaque strip. Using this model we calculate the spatial distribution of received signal intensity and phase for a variety of source-tunnel-sensor geometries, wave types (P and EM), and wave frequencies. Here we note especially the contrast between the use of EM and P waves, noting the advantages and disadvantages of each. No scattering from geological inhomogeneities is included aside from the tunnel itself.

We next discuss signal analysis schemes including matched filter and correlation detection as well as how parameter estimation might be used to obtain diagnostic information once a tunnel is detected. Observational methods vary from single source and single sensor to source and sensor arrays in three boreholes operating in a differential scheme.

The last chapter contains brief discussion of two topics. First we note that borehole to borehole tunnel detection might be accomplished by placing the line between source and sensor along the expected tunnel rather than transverse to it as discussed in Chapter III. This scheme takes advantage of the fact that the tunnel can act as a relatively low loss "waveguide" path between source and sensor. We also briefly investigate the exploration of a discovered tunnel by inserting EM or P acoustic waves directly into the tunnel. Searching for resonances in the frequency domain and radar/sonar echoes in the time domain provides information on the tunnel size, length, direction, number of bends (if any), etc.

C. Conclusions Drawn from JASON Summer Study

In our consideration of the underground propagating medium we draw several conclusions relevant to the general class of underground EM and seismic wave detection systems including both monostatic and bistatic radar type systems.

1. For frequencies of interest here inhomogeneities in the underground wave propagation medium can cause significant wave scattering as a signal propagates from source to sensor. For weathered granite, which

is typical of the Korean demilitarized zone, and typical operating frequencies (VHF for EM waves and 500-2000 Hz for P waves) a single weathered joint (crack) can reflect up to about 30% of the normally incident EM wave power and up to 90% of the normally incident P wave power.

2. Strong scattering within the propagating medium implies that clutter (signals propagating from source to sensor along unwanted paths) will be an important factor in detection system design and operation. Placement of sources and sensors at some depth below the surface by means of boreholes not only helps reduce clutter, but also reduces signal loss since path lengths are shorter. The use of polarized EM or shear wave signals may be helpful in clutter reduction.

3. In almost any detection system and certainly in the generalized radar type schemes investigated here, a careful review of the geological setting will be quite helpful in choosing the type of detection system most likely to yield successful results.

Narrowing our consideration to borehole to borehole schemes using electromagnetic (EM) or compressional seismic (P) waves we reach the following conclusions:

a. A forward scatter scheme in which one observes the signal amplitude and/or phase of the shadow diffraction pattern (or possibly forward scatter enhancement) of the tunnel seems likely to provide a workable tunnel detection system. However, inhomogeneities in the

underground medium are likely to generate a significant false alarm problem.

b. Depending on the relative accuracies of phase and amplitude measurements which can be obtained with given observational hardware. it is quite possible that phase measurements, rather than amplitude, will produce the most salient tunnel signature. It is also possible that the phase signature of a tunnel could prove relatively less susceptible to clutter from underground inhomogeneities.

c. Although subject to uncertainties in source and sensor technology as well as ambient noise levels, we conclude that P waves are likely to provide better system performance than EM mainly because P wave attenuation is so much lower in all the geological settings considered here.

d. In system design one must compromise between wanting high operating frequencies to obtain salient tunnel signatures and wanting low operating frequencies to reduce propagation losses. For the scheme considered here operating frequencies in the VHF range for EM waves and 500-5000 Hz for P waves appear practical.

e. Since real tunnels are of irregular shape with rough boundaries, accurate modeling of their scattering characteristics is very difficult. We argue on theoretical grounds that a simple model in which the tunnel is represented as an opaque diffracting strip adequately

portrays most of the important features of the tunnel's shadow diffraction pattern.

f. Because the shadow diffraction pattern is most evident when the tunnel is located near the sensor borehole, it would be advisable to make observations both before and after exchanging source and sensor boreholes.

g. Although requiring movement of both source and sensor, observations in which the source and sensor are kept at equal depths offer the advantages that interpretation is more simple and transmission losses are minimized by keeping path lengths short.

h. At the expense of increased system complexity arrays (strings) of sources and/or sensors could provide advantages in terms of beam forming and rapid data collection. However, if both signal amplitude and phase (relative to the source) can be observed at each array location by a single source-sensor pair, results equivalent to arrays can be obtained though requiring more time and manpower.

i. Again at the expense of additional system complexity matched filter, correlation detection or tomographic reconstruction schemes in the spatial domain could enhance the probability of detection while parameter estimation techniques could yield diagnostic information such as tunnel size and location.

j. A differential scheme involving a source in a central borehole with sensors in boreholes to either side could be useful in removing the effects of large scale horizontally stratified geological inhomogeneities.

Finally, there are two conclusions which arise from our brief consideration of other tunnel detection and exploration schemes:

k. It appears feasible to exploit the linear aspect of a tunnel, detecting it as a relatively low loss "waveguide" by borehole to borehole sounding along the direction of the expected tunnel rather than transverse to it as discussed above.

l. Once a tunnel is located, electromagnetic or acoustic waves could be introduced into the tunnel to explore it in terms of length, corner locations, diameter, human activity and so forth by observing radar/sonar echo time delays and doppler shifts as well as resonances in the frequency domain.

II. CHARACTERISTICS OF THE PROPAGATING MEDIUM

Clearly the propagation characteristics of the medium in which a tunnel exists will exert a great influence on the effectiveness of a given detection technique. The phase velocity will control the wavelength in the medium and thus the tunnel's resonant frequency (tunnel circumference~ wavelength). The attenuation and scattering properties of the medium limit the path lengths one may use. Indeed, inhomogeneities may strongly scatter the probing waves and even mimic tunnels.

The geological circumstances in which tunnels of interest may exist are extremely varied. We have focused our attention on a particular geologic setting common along the DMZ in Korea, namely weathered granite. Conclusions drawn from this example are, of course, not general and techniques which seem less effective in this setting may indeed be valuable elsewhere.

A. Electrical and Seismic Properties of Homogeneous Granite and Other Materials

1. Electrical Properties

Basic electrical measurements on a core sample of Korean granite were made by Dolphin (Stanford Research Institute, 1976a) from 0.5 to 250 MHz. The sample was obtained from a borehole near the Sobang-San tunnel mentioned in the introductory section above. Since the sample was

not received in a moisture-tight container, it was measured in water-saturated and oven-dried states as well as "as received." The results are reproduced in Fig. 1 for convenience. It is immediately evident that for frequencies near tunnel resonance (~ 30 MHz) attenuation will be relatively high (~ 0.1 to 1 dB/m). Since granite in the Korean DMZ setting is likely to be near the water-saturated curve and radar system dynamic range is at most about 100 dB, path lengths will be limited to about 100m. As Dolphin (1976) points out, this implies that the use of surface electromagnetic wave radars for the location of deep tunnels will be severely limited.

Although there has been considerable research into the electrical properties of geologic materials in general (Watt, et al., 1963; Keller and Frischknecht, 1966; Parkhomenko, 1967; Wait, ed., 1971), the emphasis has been on measurements at low frequencies (less than a few hundred kHz). Measurements at higher frequencies are generally of more recent vintage (Gates and Armistead, 1974; Cook, 1975a and b; Vickers, 1976). For comparison, we show in Fig. 1 the electrical properties of a sample of Oregon sandstone (Vickers, 1976). It is evident that in both cases the attenuation factor (α) and the dielectric constant (ε_r) rise substantially when water is present. This is not surprising when one considers the very high values of ε_r and α characteristic of water solutions involving common minerals, e.g., sea water (Kraichman, 1970).

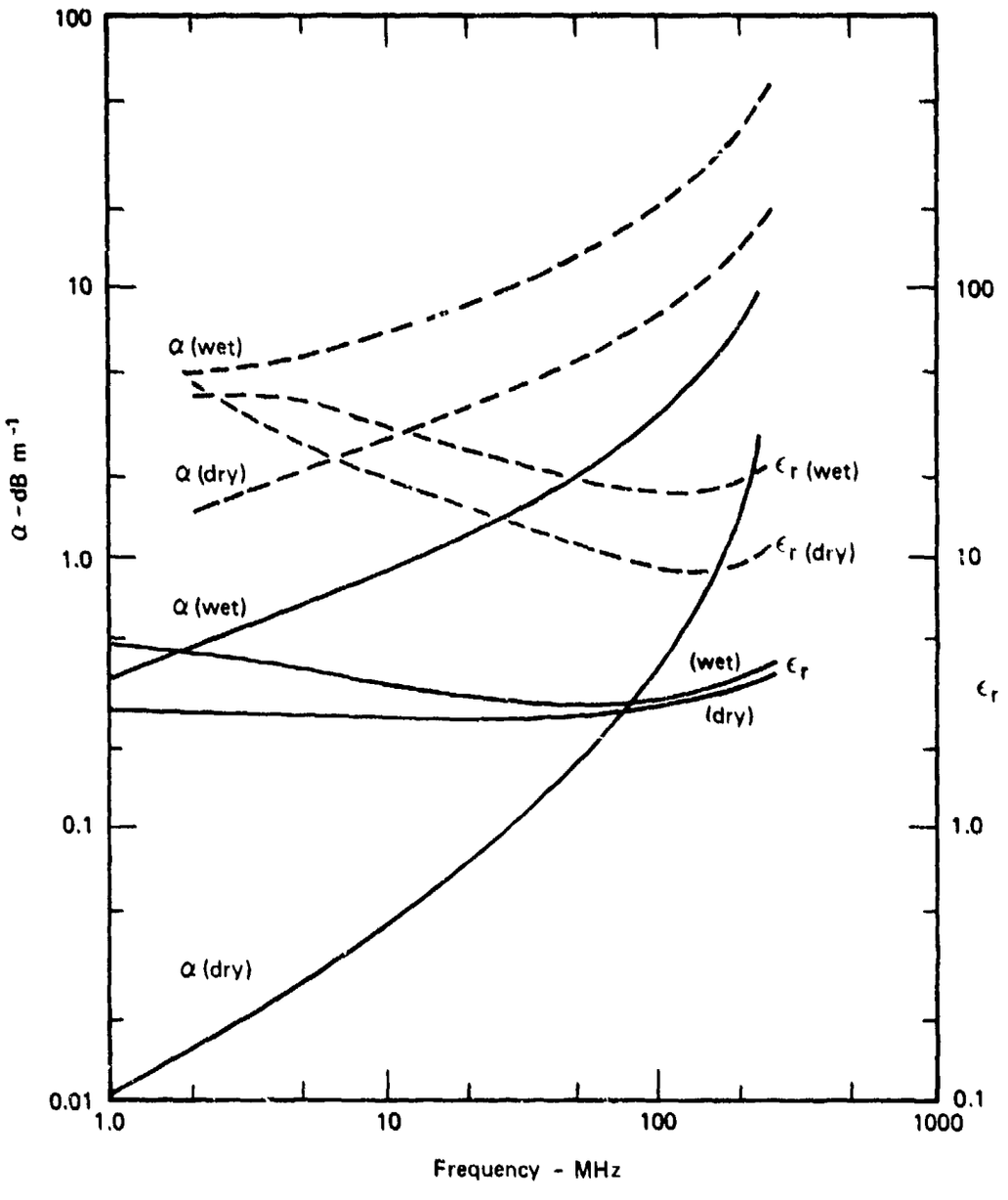

Figure 1. Measured dielectric constant (relative permittivity) ϵ_r and attenuation coefficient α for Korean Granite (solid lines) and Oregon Sandstone (dashed lines). Curves are drawn for both oven dried and water saturated states in order to show the wide range in the measured parameters as a function of water content. The sources for these measurements were (DOLPHIN, 1976) for the granite and Figure 21 of (VICKERS, 1976) for the sandstone.

2. Seismic Properties

The propagation of seismic (elastic) waves in geologic materials is a complex subject (see, for example, Ewing, et al., 1957: White, 1965; and Officer, 1974). In an isotropic solid only two types of seismic waves are found: P (compressional) and S (shear) corresponding to longitudinal and transverse material motion respectively. However, when one considers a realistic situation in which boundaries between elastic media exist, a third kind of wave, known as a Rayleigh wave, can propagate along the boundary (e.g., at a free surface). Further, a fourth type of wave, known as a Love wave, can propagate along a boundary if one considers layers rather than simply boundaries, e.g., Love waves can propagate along the Earth's surface if the velocities of P and S waves increase with depth below the surface.

The phase velocity of a P wave (c_P) is given by

$$c_P = \sqrt{\frac{K + (4\mu/3)}{\rho}}$$

where K is the bulk modulus, μ is the rigidity or shear modulus and ρ is the density (all in cgs units). The phase velocity of S waves is given by

$$c_S = \sqrt{\mu/\rho} \quad .$$

White (1965, Ch. III) discusses the loss mechanisms and attenuation of seismic waves in homogeneous rock. Following his treatment

we will characterize the losses as follows:

$$A_i(x) = A_{oi} \exp\left[-a_i x + j(k_i x - \omega t)\right]$$

where A_i is the wave amplitude in the ith mode of a wave propagating in the positive x direction. The loss parameter for the ith mode is a_i; loss parameters for both $i = P$ (compressional) and $i = S$ (shear) waves are given for several rock types in Table 1.

Since we are seeking to detect tunnels by propagating waves through bulk material, our primary interest is in compressional and shear waves and we shall only consider them for the most part. However, Rayleigh and Love waves can propagate unwanted signals from a seismic source to a receiver. Also, there is the possibility of significant wave coupling at the interfaces in an inhomogeneous medium. For example, a compressional wave upon striking an interface transfers some of its energy into reflected and refracted waves in both P and S modes and possible surface wave modes as well, depending on the circumstances. Officer (1974, section 6.3) gives an introductory discussion of the reflection and refraction of seismic waves at a plane boundary. The problems associated with such wave coupling are too varied and complex to be treated here, though they may indeed have importance especially for propagation in an inhomogeneous medium.

TABLE 1

Seismic Properties for Several Rock Types

ROCK TYPE	c_P (km s^{-1})	c_S (km s^{-1})	f (Hz)	a_P (cm^{-1})	a_S (cm^{-1})	COMMENTS
Granite (in general)*	4.6 to 7.0	2.5 to 4.0				
Granite (specific samples)**						
Kamyk	6.1	3.5	$(0.2 \text{ to } 2) \times 10^6$	$3.9 \times 10^{-8} f$		1
Sample 3	5.5	3.3	$(30 \text{ to } 180) \times 10^3$	$2.7 \times 10^{-7} f$	$3.3 \times 10^{-7} f$	1
Sample 4	4.9	3.0	$(30 \text{ to } 180) \times 10^3$	$1.4 \times 10^{-7} f$	$1.7 \times 10^{-7} f$	1
Quincy	4.3	2.8	140 to 4,500	$4 \text{ to } 7 \times 10^{-8} f$		2
Limestones and dolomites (in general)*	3.5 to 6.5	1.8 to 3.8				
Limestones (specific samples)**						
Solenhofen	5.6	2.9	$(3 \text{ to } 15) \times 10^6$	$5.2 \times 10^{-8} f$	$5.8 \times 10^{-8} f$	1
Sample I-1	6.1	3.2	$(3 \text{ to } 15) \times 10^6$	$3.1 \times 10^{-8} f$	$\approx 2.5 \times 10^{-8} f$	1
Hunton			$(3 \text{ to } 10) \times 10^3$	$1.2 \times 10^{-7} f$		2
Sandstones (specific samples)**						
Sample 116	5.0		10^6	0.035 cm^{-1} @ 10^6 Hz		1
Amherst			900 to 1,300	$2.7 \times 10^{-7} f$		2
Chalk (specific samples)**						
Chislehurst	2.3	1.2	600	$6 \times 10^{-6} \text{ cm}^{-1}$ @ 600 Hz		3
Shale (specific samples)**						
Sylvan			$(3 \text{ to } 12) \times 10^3$	$1.2 \times 10^{-7} f$		2
Pierre	2.2	0.81	50 to 450	$4.5 \times 10^{-7} f$		3
Pierre			20 to 125		$4 \times 10^{-6} f$	

See Notes to Table 1

NOTES TO TABLE 1

* Data taken from Parasnis (1972, Ch. 6)

** Data taken from White (1965, Ch. 3)

1 Laboratory measurement

2 Laboratory measurement applicable to longitudinal waves governed by Young's modulus

3 Bulk medium measured in field experiment

There are a number of reasons why compressional (P) waves are of dominant importance in applied seismology. To begin with, S waves are difficult to generate with sufficient intensity. Explosives generate predominantly, if not exclusively, P waves (Parasnis, 1972, Ch. 6). Secondly, a perusal of Table 1 shows that S waves are almost always more strongly attenuated than P waves. Though the difference may be small, it is in the exponent and hence important. For these reasons we shall concentrate on the more widely used P waves in the discussions which follow.

B. Propagation Characteristics Typical of Weathered Granite

1. Weathering of Granite

The near surface granite rock found in a natural setting will contain various inhomogeneities. The ones of most interest here are those introduced by the geological process of weathering. Since these inhomogeneities imply corresponding variations in the refractive index for both seismic and electromagnetic waves, it is important to know what factors control the weathering process and the sort of inhomogeneities typically found in weathered granite. The brief discussion of these questions set out below is drawn principally from Fett (1976) with supplementary material from Ollier (1969) and Kerhoogan (1970).

Most generally, weathering is the process by which near-surface materials are changed so as to bring them more nearly into equilibrium with a new physical, chemical and biological environment.

Granite is, in general, a plutonic rock, i.e., an igneous rock, formed by the solidification of magma under great pressure deep within the Earth. When this solidified material is transported to locations near the Earth's surface, the pressure is greatly reduced and the resulting internal stresses cause the rock to fracture. Such fractures are known geologically as joints. Typically these joints form along sets for fairly well defined and approximately parallel planes. The separation between planes ranges from fractions to five or more meters and there are usually two or more sets of planes having different orientations. One of these sets of planes is typically approximately parallel to the local surface and results in sheets of rock following the local topography and increasing in thickness with depth. In Figs. 2 and 3 we see how the horizontal sheets combined with sets of near vertical joints can cut basement rock into blocks.

Weathering proceeds mainly along these joints since they provide pathways for water solutions to flow deep within the rock and attack it chemically and mechanically. To begin with, rainwater itself is slightly acidic (pH = 6-7) because of dissolved O_2 and CO_2, and this acidity may be enhanced as the water percolates down through layers of rotting vegetation. Once this acidic solution comes in contact with the rocks along the joints, it begins to react chemically with the mineral constituents of granite. Typically, granite is composed mainly of feldspar, mica and quartz (in order of vulnerability to weathering). The quartz remains unaltered, but the feldspars and micas are usually converted to softer clay minerals such as kaolinite. The boundary between the weathered and unweathered rock is usually well defined in granite, being a few mm or less.

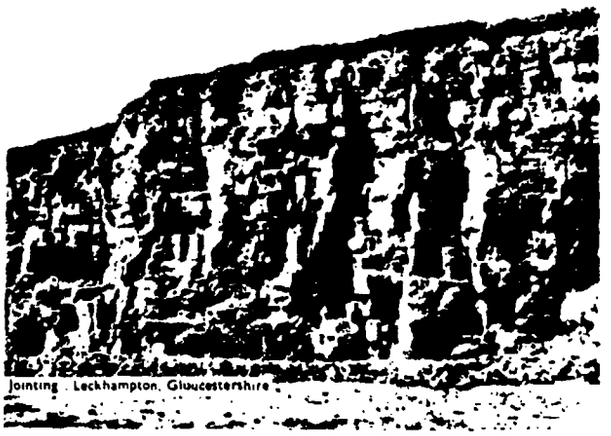

Figure 2. Illustration of basement rock being cut into blocks by horizontal and vertical jointing planes. This example is taken from Salterley Grange Quarry, Leckhampton Hill, Gloucestershire, UK. where prominent vertical joints cut through oolitic limestone. (Photo courtesy of the Geological Survey and Museum, London).

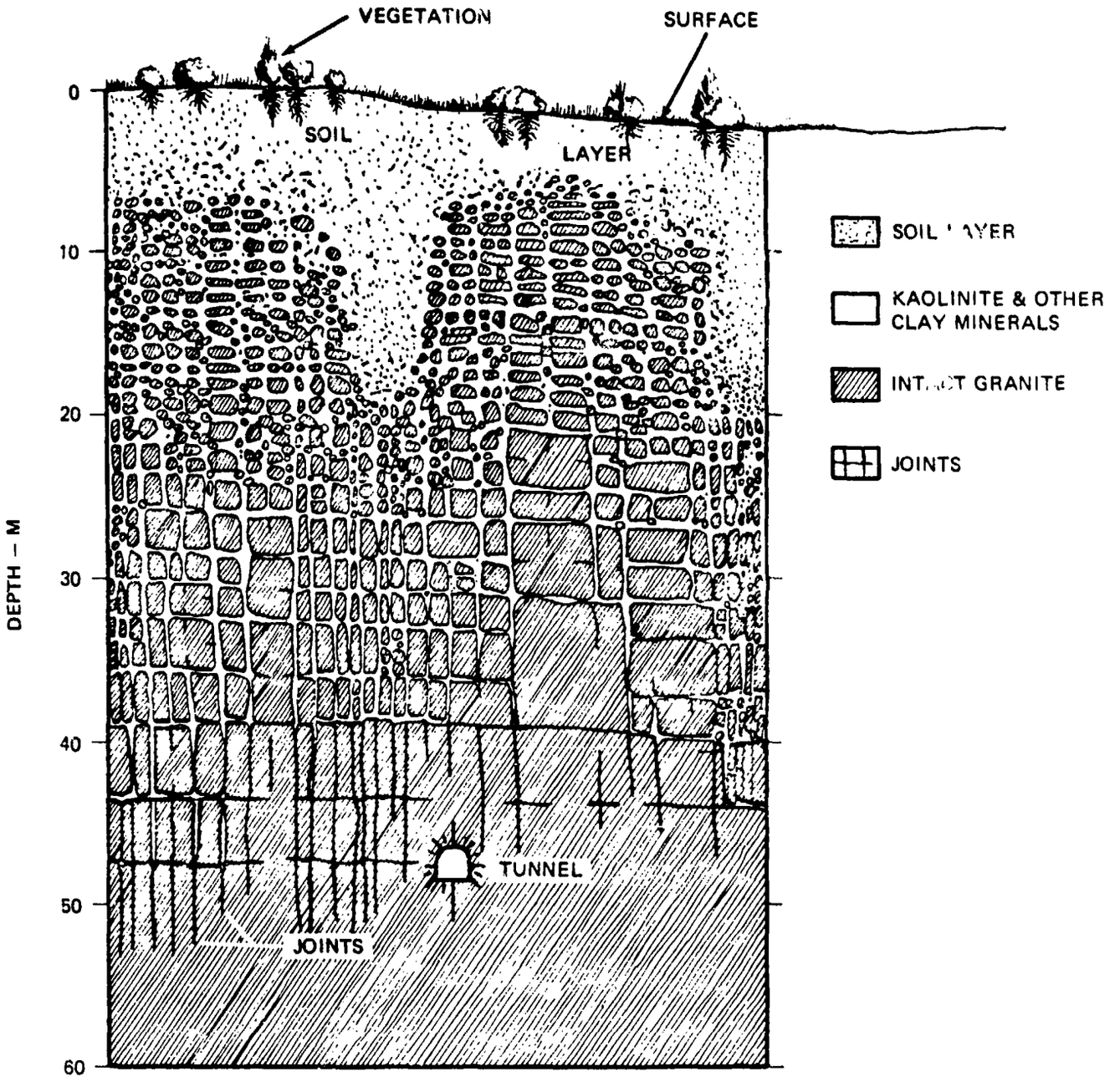

Figure 3. SCHEMATIC REPRESENTATION OF WEATHERED GRANITE. NOTE INCREASING SIZE AND FRACTION OF INTACT GRANITE BOULDERS. KAOLINITE AND OTHER CLAY MINERALS, WHICH RESULT FROM THE WEATHERING OF GRANITE, FILL THE SPACES BETWEEN BOULDERS. IN A NATURAL SETTING THE JOINTING PLANES COULD WELL BE IN DIRECTIONS OTHER THAN HORIZONTAL AND VERTICAL, AND MORE THAN TWO SETS OF PLANES COULD EXIST.

Mechanical disintegration can also result from water penetration along joints. If water freezes at atmospheric pressure, its volume increases by about 11%. The weathering produced by the expansion and contraction of repeated freezing and thawing is called frost riving and would certainly be active along the Korean DMZ.

As weathering proceeds, joints become wider and filled with clay. In general, weathering attacks sharp edges most strongly, and as joint blocks become isolated by intervening clay they weather into spherical shapes. Sometimes these roughly spherical granite boulders will become case hardened and resist further weathering. Case hardening occurs when silica and hydrated oxides of iron, manganese and aluminum precipitate from surface water along the surface of a rock. These materials, once they precipitate from solution do not redissolve and thus protect surface materials, inhibiting further weathering.

A question of particular interest in the present case is how deep weathering effects extend. Although the question must be answered for each location separately, it is known that weathering of granite can extend to large depths. For example, Ollier (1969, p. 121) reports weathering in granite to maximum depths of 37, 45, 70 and 274 meters at four well separated locations in Australia. In general terms, weathering extends to greater depths in regions where precipitation, vegetation and temperature fluctuations (across the freezing point of water) are maximized. Thus weathering extends to large depths (tens of meters) in tropical rain forest and temperate regions, but to only small depth (meters) in low-latitude desert and arctic regions (Hamblin, 1975, pp. 120-129).

2. Present Condition of Weathered Granite

The question now arises as to what a weathered granite environment might look like at the present time. Such a picture, uncertain though it may be, gives one at least some guidance in assessing the effects of an inhomogeneous medium on seismic and electromagnetic wave propagation, i.e., how much attenuation one might expect from wave scattering and how bad the clutter problem will be. In Fig. 3 we have drawn a schematic representation of what weathered granite might look like at the present time. This picture is based principally on the following sources: Fett (1976), Hamblin (1975) and Ollier (1969); and is, of course, only an estimate of what an actual structure might look like. However, the picture does contain most of the salient features commonly found in weathered granite. The jointing structure, shown in Fig. 3 as sets of roughly parallel vertical and horizontal planes, may vary considerably in the natural environment. Usually the joints are along several relatively well defined sets of parallel planes with one set of planes roughly parallel to the local surface. Other jointing planes are often roughly vertical as shown in Fig. 2, but are also found to run at oblique angles to the local vertical. Below the soil layer we find solid granite boulders surrounded by softer clay minerals such as kaolimites, the clay minerals being the results of the chemical weathering of granite. The size and fraction of granite boulders increases with depth finally approaching homogeneous granite at sufficient depth.

3. Variations in the Electrical and Seismic Properties between Homogeneous and Weathered Material

We have now established that in a weathered geological setting interfaces between the parent (homogeneous) and the weathered material are common. Further, in the case of weathered granite the interface between the parent granite and the weathered clay is likely to be relatively sharp (Ollier, 1969, p. 121). In order to estimate the effects such interfaces may have on electromagnetic and seismic wave propagation, it is necessary to know the variation in wave propagation parameters across such interfaces. We will simplify a typical situation somewhat by assuming granite to be the only parent material and clay minerals to be the only weathering product. The required parameters are given in Table 2. For simplicity and other reasons discussed in section C below, we consider only compressional seismic waves. Our objective here is to obtain an estimate of the power reflected from such a joint. The reflected power would contribute to the clutter and signal loss for both monostatic (colocated transmitter and receiver) and bistatic (separated transmitter and receiver) underground radar/sonar systems.

TABLE 2

Approximate Propagation Parameters* for Electromagnetic and Compressional Seismic Wave in Granite and Clay

PARAMETER*	GRANITE	CLAY
Electromagnetic Waves:		
f = 30 MHz		
ε_r	3.1 (1)**	10 (2)
α	1.4 db m^{-1} (1)	5.0 db m^{-1} (2)
f = 60 MHz		
ε_r	2.9 (1)	8.7 (2)
α	2.2 db m^{-1} (1)	7.6 db m^{-1} (2)
f = 120 MHz		
ε_r	2.8 (1)	7.6 (2)
α	4.1 db m^{-1}	12 db m^{-1} (2)
Compressional Seismic Waves:		
f = 500 Hz		
c_p	5×10^3 ms^{-1} (3)	2.3×10^3 ms^{-1} (5)
a_p	1×10^{-2} m^{-1} (4)	5×10^{-4} m^{-1} (5)
f = 1000 Hz		
c_p	5×10^3 ms^{-1} (3)	2.3×10^3 ms^{-1} (5)
a_p	2×10^{-2} m^{-1} (4)	1×10^{-3} m^{-1} (5)
f = 2000 Hz		
c_p	5×10^3 ms^{-1} (3)	2.3×10^3 ms^{-1} (5)
a_p	4×10^{-2} m^{-1} (4)	2×10^{-3} m^{-1} (5)

NOTES TO TABLE 2

* ε_r = relative permittivity = dielectric constant

α = attenuation coefficient for power (db m^{-1})

c_p = compressional seismic wave velocity

a_p = compressional seismic wave attenuation coefficient for amplitude (m^{-1})

** Numbers in parentheses indicate sources of information listed below.

SOURCES: (1) Water saturated curve from (Dolphin, 1976), see Fig. 1.

(2) The relative dielectric constant and conductivity data given by Hipp (1974) for "grey San Antonio clay loam" at 1800 kg m^{-3} dry density and 2.5% moisture are used. Since $\sigma/\omega\varepsilon \gtrsim 1$, the attenuation was computed using the complete expression from Kraichman (1970, p. 2-1) rather than the convenient approximation for a poor conductor ($\sigma/\omega\varepsilon \ll 1$) , i.e.,

$$\alpha = 8.69\omega \left\{ \left(\frac{\mu\varepsilon}{2} \right) \left[\left(1 + \frac{\sigma^2}{\omega^2 \varepsilon^2} \right)^{1/2} - 1 \right] \right\}^{1/2} \text{db m}^{-1}$$

in S.I. (mks) units. The difference between the two was in fact less than 3%.

(3) Average of 5 granite samples collected by White (1965, p.89) from several sources.

(4) Average of 2 granite samples collected by White (1965, p. 89) from two sources.

(5) Chislehurst chalk measured in bulk at 600 Hz (White, 1965, p. 89) and extrapolated linearly with frequency.

The problem of calculating the reflection coefficient for power ($|\rho|^2$ = power in reflected wave/power in incident wave) is solved by Ramo, et al., (1965, pp. 349-351). The result for $|\rho|^2$ as observed in medium 1 (on the left in Fig. 4) is given for normal incidence by

$$|\rho|^2 = \left| \frac{Z - \eta_1}{Z + \eta_1} \right|^2 \tag{1}$$

where

$$Z = \eta_2 \frac{\eta_1 \cos(k_2 \ell) + j\eta_2 \sin(k_2 \ell)}{\eta_2 \cos(k_2 \ell) + j\eta_1 \sin(k_2 \ell)} \quad .$$

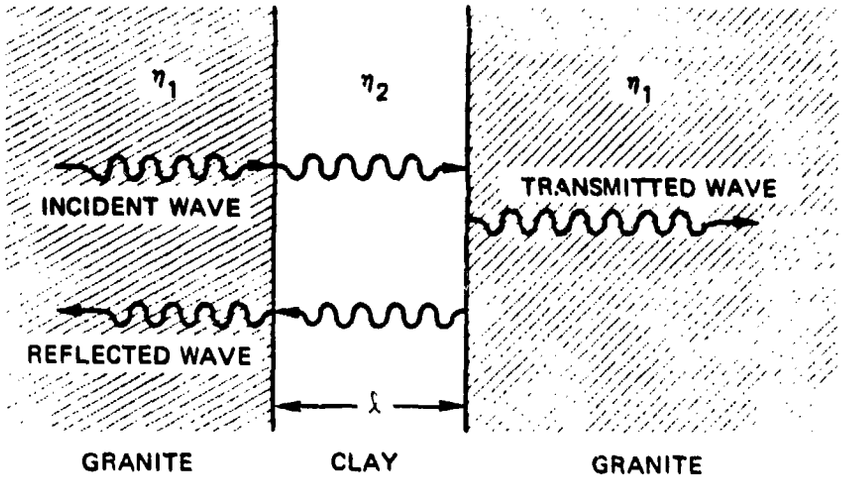

Figure 4. A SIMPLE SLAB MODEL FOR PROPAGATION ACROSS A WEATHERED JOINT (AFTER RAMO et. al., 1965)

In the case of electromagnetic waves

$$\eta_i = \sqrt{\mu_i/\epsilon_i} \quad ,$$

with μ_i and ϵ_i being the permeability and permittivity of the ith medium, and

$$k_2 = 2\pi/\lambda_2 \quad ,$$

$\lambda_2 = 1/\left[f\sqrt{\mu_2\epsilon_2}\right]$ being the wavelength in medium 2, the clay of Fig. 4.

In the compressional seismic (P) wave case

$$\eta_j = \rho_j c_{Pj}$$

where ρ_j and c_{Pj} are the density and the compressional seismic wave velocities in the jth medium and

$$k_2 = \frac{2\pi f}{c_{P2}}$$

In the seismic wave case one must be rather cautious because shear (or S) waves as well as compressional (or P) waves can propagate in an elastic medium. Moreover, when compressional waves strike an interface away from normal incidence, shear waves are generated on both sides of the interface. The case considered here of a compressional wave normally incident on an interface is particularly simple since no shear waves are generated

(Telford, et al., 1976). In most geological settings the amount of reflected and refracted power going into shear waves is relatively small and can be neglected for angles of incidence less than about 20°. Telford, et al., consider an illustrative example showing the relative amounts of energy going into reflected and refracted, compressional and shear waves as a function of angle of incidence and other parameters.

For the case where $k_2 \ell << 1$ we may use a first order approximation to Z above and $|\rho|^2$ becomes

$$|\rho|^2 \approx \frac{k_2 \ell}{2} \left| \frac{\eta_1}{\eta_2} - \frac{\eta_1}{\eta_2} \right|^2 \quad . \tag{2}$$

In Figs. 5 and 6 we have plotted $|\rho|^2$ for both electromagnetic and seismic waves [calculated according to Eq. (1) or (2)] as a function of joint width ℓ for several frequencies. The EM and seismic wave frequencies in Figs. 5 and 6 correspond in the sense that each pair of frequencies has the same wavelength in granite. For example, 30 MHz EM waves and 900 Hz P-waves both have wavelengths of about 6 m in granite. This correspondence has been introduced so that one can compare the reflection properties of the two types of waves, each of which will interact in approximately the same fashion with a tunnel. In the left-hand portion of the figure $k_2 \ell << 1$ and $|\rho|^2$ becomes proportional to ℓ^2 as indicated in Eq. (2). In the right-hand portion of the figure, $k_2 \ell$ becomes comparable to unity and a pattern of periodic nulls appears as

indicated in Eq. (1). A number of implications for tunnel detection arise from even this crude model; however, we will defer discussion of them to Section C below.

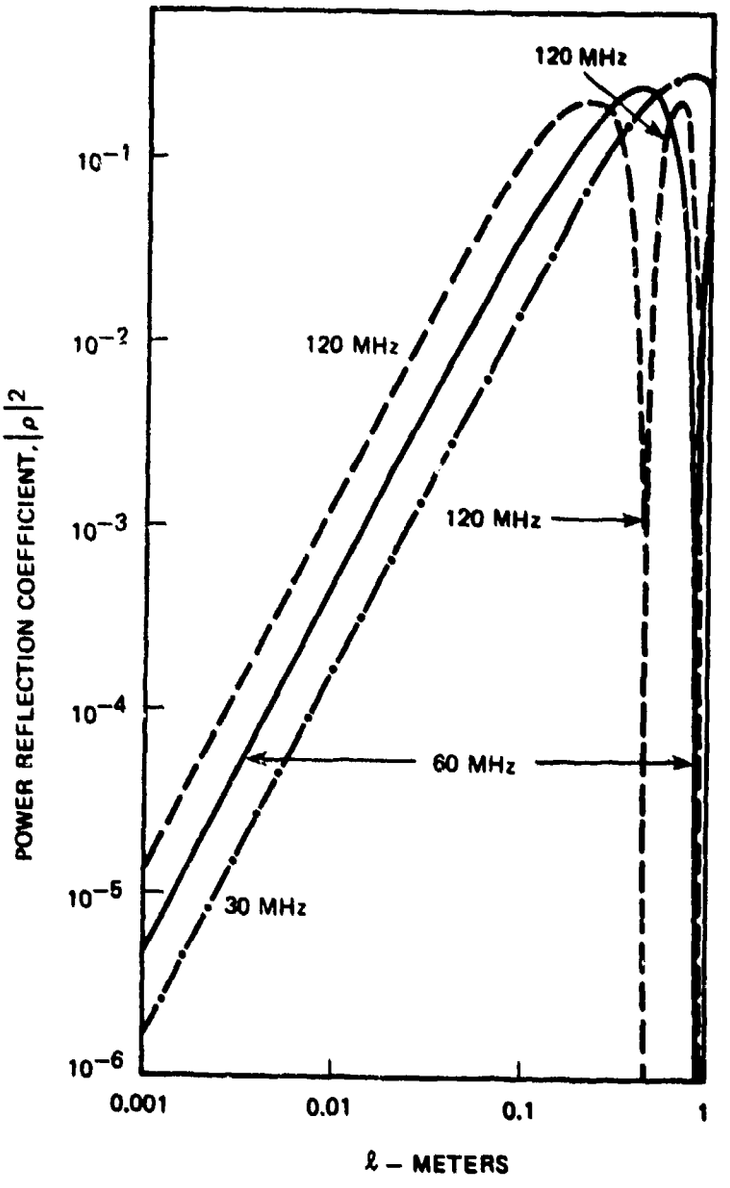

Figure 5. POWER REFLECTION COEFFICIENT $|\rho|^2$ AS A FUNCTION OF JOINT WIDTH ℓ FOR THREE ELECTROMAGNETIC WAVE FREQUENCIES.

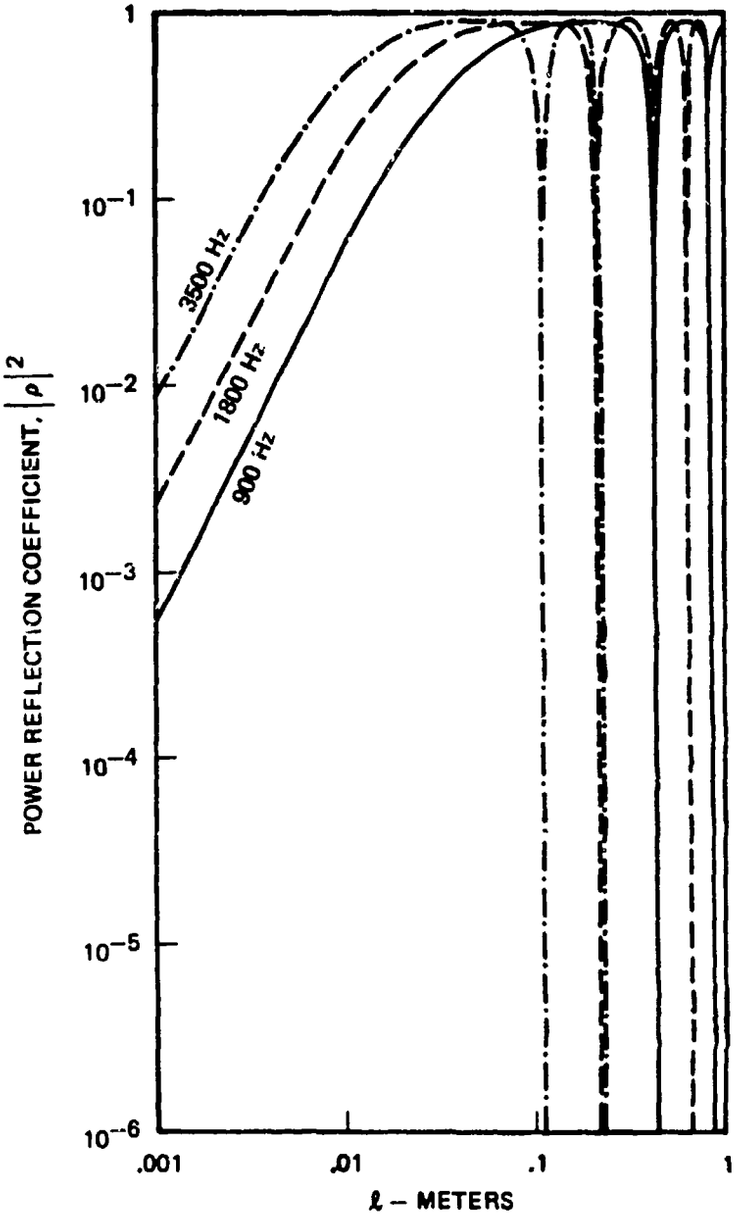

Figure 6. POWER REFLECTION COEFFICIENT $|\rho|^2$ AS A FUNCTION OF JOINT WIDTH ℓ FOR THREE COMPRESSIONAL SEISMIC WAVE FREQUENCIES. THESE FREQUENCIES CORRESPOND TO THE ELECTROMAGNETIC WAVE FREQUENCIES OF Figure 5 IN THAT THE WAVELENGTHS IN THE PARENT MATERIAL (GRANITE) ARE THE SAME FOR BOTH TYPES OF WAVES. THE CURVE FOR 3500 Hz HAS BEEN DELETED FOR $\ell \gtrsim$ 0.2 m IN ORDER TO AVOID CONFUSION IN THE RIGHT–HAND PART OF THE FIGURE.

C. Implications for Seismic and Electromagnetic Sounding

1. Surface vs. Borehole Sounding

Although the use of sensors down boreholes clearly requires more effort and expense than the use of surface sensors, the substantial advantages of borehole sensors (in terms of higher probability of detection and lower false alarm rate) suggests that they be used whenever possible, especially when the search can be localized (for example, by defector information). To begin with, borehole sensors can be located closer to the suspected tunnel thus reducing propagation loss. Borehole sensors are more isolated from surface sources of interference such as electromagnetic waves travelling from source to receiver via atmospheric paths. A perusal of Fig. 3 shows that, at least in some realistic cases, unwanted reflections (clutter) from geological inhomogeneities will be a much more serious problem near the surface than at depths of a few tens of meters.

2. The Problem of Unwanted Reflections (Clutter)

The "clutter" problem proves to be quite significant since it can limit the effective range of an underground electromagnetic or seismic wave "radar". (Radar here is taken in a very general sense including pulse and continuous operation with electromagnetic or seismic waves as well as monostatic or bistatic configurations.) The clutter problem is in fact a very real problem limiting underground electromagnetic radars to a dynamic range on the order of 100 db at frequencies on the order of 10 to 100 MHz. Figs. 5 and 6 illustrate the seriousness of the clutter problem. For example, a 6 m long wave in granite (30 MHz electromagnetic or 900 Hz

compressional seismic) has a power reflection coefficient of 0.02 if electromagnetic and 0.8 if compressional seismic at a single joint containing weathered material some 10 cm wide. If one can reduce the joint width ℓ by positioning the source and sensors at greater depth, (see Fig. 3), there is likely to be substantial clutter reduction. It is important to note the obvious fact that clutter imposed limitations can not be overcome by simply increasing the source power level as would be the case in a system limited by ambient noise.

In the case of electromagnetic waves some improvement in the signal to clutter ratio can usually be obtained by taking advantage of any differences between the polarization received after scattering from unwanted as compared to desired objects. The Terrascan underground utility locator, developed by Leon Peters and his colleagues at Ohio State University (Peters, 1975) and manufactured by Microwave Associates Inc. (1976), employs a pair of orthogonally polarized, folded dipole antennas for clutter reduction. A linearly polarized signal is transmitted on one antenna and received on the other (cross-polarized) antenna. Signals reflected from plane interfaces parallel to the plane of the crossed antennas will be linearly polarized along the direction of the transmitting antenna and thus orthogonal to the receiving antenna. As seen by the receiver, such orthogonal echoes will be strongly attenuated. This type of system can clearly reduce the radar clutter due to plane, horizontal layers in the Earth. Desired non-plane objects, such as pipes, produce "depolarized" components in the reflected signal and those can be relatively easily detected using the cross-polarized receiving antenna.

However, geological inhomogeneities are not restricted to horizontal plane layers (although they tend to be horizontal near the surface) and natural interfaces are usually rough rather than plane. Such inhomogeneities produce depolarized clutter which interferes with the desired echo.

Since seismic S-waves are polarized it is conceivable that one might use S-waves in a clutter rejection scheme similar to that described for EM waves above. However, S-waves are more difficult to generate and are generally a little more strongly attenuated (see Table 1) than P-waves. In addition, there can be a strong cross coupling betwen P- and S-waves at interfaces between layers with differing seismic properties, so P-waves get converted to S-waves and vice versa. (Telford, et al., 1976, Ch. 4.) This complicates the interpretation and could be particularly important in a system relying on S-waves, since any P-waves inadvertently generated by the source could ultimately reach the detector as S-waves.

3. Electromagnetic vs. Seismic Waves

From the above discussions it is clear that either electromagnetic or seismic waves could be a logical best choice for tunnel detection work. The choice would depend on such factors as:

- the geological setting which determines the wave speed, attenuation and dispersion as well as the importance of clutter echoes;
- the probable characteristics of the suspected tunnel (e.g., does it contain steel rails?);

- o the geographical location (e.g., can boreholes be drilled?); and
- o the nature of the detection equipment available.

As an example, consider a geological setting of weathered granite as described above. We will employ a backscatter-type radar which searches for the echo reflected from the tunnel. Assume that the suspected tunnel is a cylinder, 1 meter in radius, and contains no conducting rails. Such rails would, of course, be of distinct advantage to EM wave techniques. We will use a wavelength of 6 meters, approximately equal to the tunnel circumferences, so that the probing wave resonates with the tunnel. In granite this implies electromagnetic (EM) and seismic wave frequencies of about 28 MHz and 800 Hz respectively. From Table 2 we note that in granite the EM wave propagation loss is substantially higher: 1.4 db/m as compared to about 0.4 db/m for P-waves. In the weathered, clay material the EM wave attenuation becomes substantially greater (5 db/m), while the P-wave attenuation is in fact greatly reduced (0.003 db/m). Clearly the EM waves will suffer greater propagation loss, but we must also know the source strength as well as the background noise level against which detection must be made in each case. In both the EM and seismic cases detection will most probably have to be made against a background of unwanted reflections (clutter) rather than an ambient noise background. A perusal of Figs. 5 and 6 shows that clutter is likely to be significantly less severe in the EM case since EM waves are less strongly reflected at joint interfaces than are seismic P-waves. By the same token, according to Eq. (1), the reflection of P waves at a tunnel's granite/air interface will

be virtually complete, whereas EM waves will be reflected with an efficiency of about 40%. Electromagnetic waves offer the possibility of at least some clutter rejection by the use of polarization discrimination, whereas P-waves are not polarized and S-waves, though polarized, are difficult to use as noted above. The resolution in range with which one could locate the tunnel, once detected, is about the same for either electromagnetic or P-waves (~10 m). Since the several factors considered do not consistently favor either choice, a more detailed analysis, tailored to a particular geological setting and including hardware and background noise considerations, would be necessary before a definitive choice could be made.

This example clearly illustrates the need for a careful analysis of the medium in which the tunnel is bored before an effective detection technique can be selected. Geological settings vary greatly, even over relatively short distances; thus considerable geological expertise is required to choose the appropriate methods and effectively interpret the data. For the same reason, automated data interpretation is of limited use and must be very flexible. Automated data collection and the display of this data in a "convenient form" is, of course, clearly useful. This convenient form may, in fact, require considerable data processing.

III. TUNNEL DETECTION USING FORWARD SCATTER BETWEEN BOREHOLE SIGNAL SOURCES AND SENSORS

A. Data Collection Scheme

In Fig. 7 we illustrate the sensor geometry. Here one or more seismic or electromagnetic sources are placed along borehole A with a string of receiving sensors along borehole B . A single source and a single sensor could also be used by moving them up and down their respective boreholes. The data collection and analysis van contains apparatus for controlling the sources and recording data (via cables), as well as on site analysis. At each sensor the vector sum of direct and scattered continous wave signals is received. Both the phase and amplitude of the received signals would be recorded. It was pointed out in Section II that weathered material typically contains many features capable of scattering quite significant amounts of power. Thus we have shown scatter paths involving geological inhomogeneities as well as the suspected tunnel.

If we consider a tunnel as simply a cylindrical scattering object, it is clear (e.g., see Ruck, et al., 1970, Ch. IV) that much of the scattering (diffraction) phenomena, which we will find useful in detecting and characterizing a tunnel, are best observed in or near the forward scatter direction (namely, the diffraction shadow of the tunnel or forward scatter enhancement). Hence we will consider primarily a detection geometry in which forward scattering from the suspected tunnel can be observed. This approach uses spatial variations in the scattered signal. One might also use variations in the source frequency.

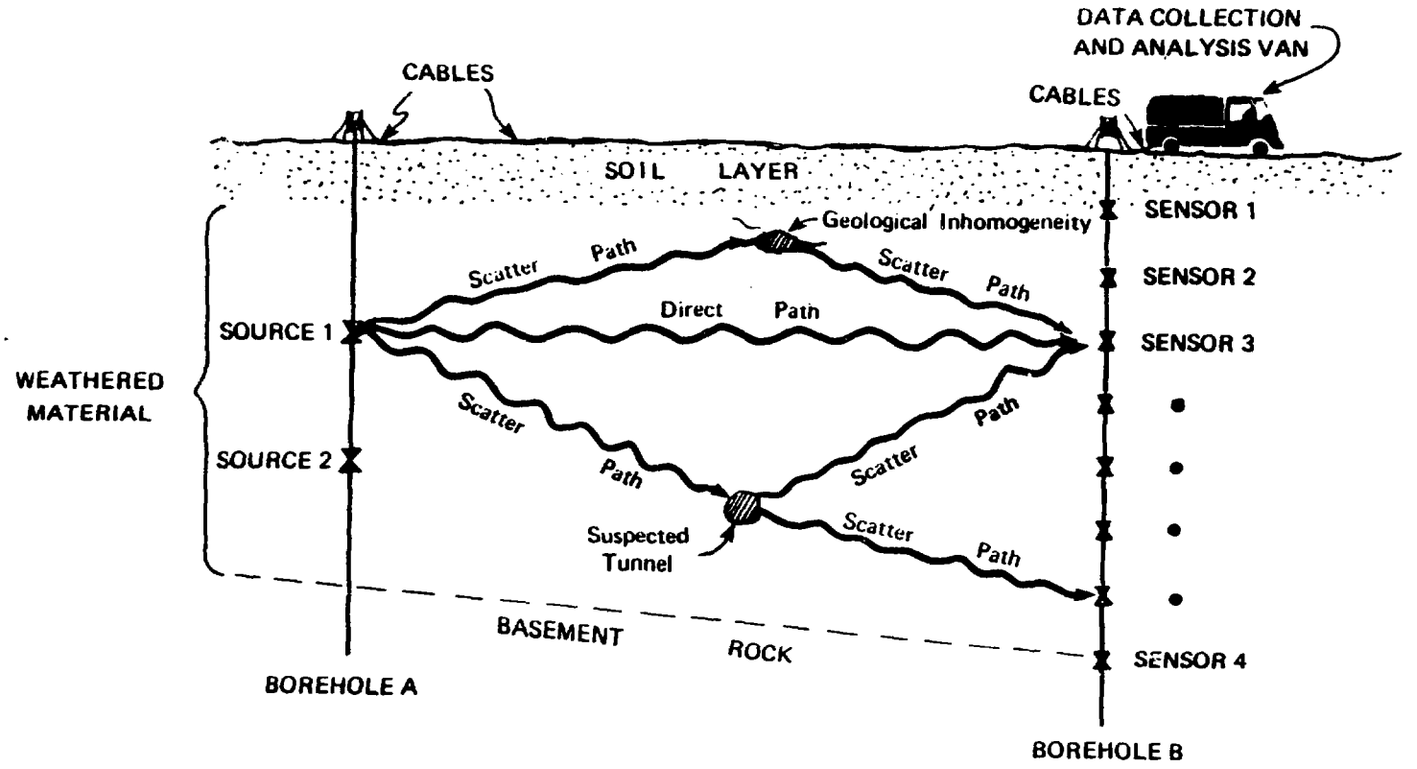

Figure 7 SENSOR GEOMETRY FOR TUNNEL DETECTION USING FORWARD SCATTER BETWEEN BOREHOLE SENSORS. TO CLARIFY THE FIGURE WE HAVE NOT SHOWN GEOLOGICAL STRUCTURE, SUCH AS WEATHERED JOINTS, WHICH COMPLICATE THE PROBLEM. Figure 3 ABOVE GIVES A SCHEMATIC REPRESENTATION OF WHAT WEATHERED MATERIAL CAN BE LIKE.

B. Forward Scatter by a Cylindrical Object

1. Wave Transmission and Reflection at the Tunnel Walls

Since a tunnel is aptly characterized as the absence of rock (or earth), it is important to ask how efficiently the interface at the tunnel wall transmits or reflects incident waves. To obtain an approximate answer consider a simple slab model for the tunnel as illustrated in Fig. 4 above. In this approximation the tunnel is just an air gap of thickness ℓ between two slabs of rock. We see from the equations following Fig. 4 that the power reflection coefficient $|\rho|^2$ is dependent on the characteristic impedances of the air in the tunnel η_2, and of the surrounding material η_1 as well as the product $(k_2\ell)$ of the tunnel width and radiation wave number in air, i.e., the width of the tunnel in wavelengths.

A brief examination of Eq. (1) reveals that for given values of η_1 and η_2, $|\rho|^2$ varies dramatically with $k_2\ell$, i.e., with tunnel width as measured in radiation wavelengths (λ_{air}) across the tunnel. For small values of $k_2\ell$, narrow tunnels and long wavelengths, $|\rho|^2$ is proportional to $(k_2\ell)^2$ as shown in Eq. (2). As $k_2\ell$ increases, a maximum is reached when $k_2\ell = \pi/4$, i.e., when the tunnel width ℓ equals $\lambda_{air}/4$. Further increases in $k_2\ell$ produce additional broad maxima at odd multiples of $\lambda_{air}/4$ separated by narrow nulls at even multiples of $\lambda_{air}/4$. Figures 5 and 6 above illustrate the general features of the variation of $|\rho|^2$ with $k_2\ell$. So long as $k_2\ell$ is not $\ll 1$ or near even multiples of $\lambda_{air}/4$, one can expect a reflection

coefficient not far below the maximum value. For a real tunnel, nulls and maxima would be somewhat displaced from the slab model values, but the general behavior is similar (see report by Peters, et al., in Stanford Research Institute, 1977).

Let us now look further at this maximum value of $|\rho|^2$ for tunnels in various geological material and for both electromagnetic (EM) and compressional seismic (P) waves. Evaluating Eq. (1) for $k_2 \ell = \pi/2$ we find that the maximum value of $|\rho|^2$ can be written in terms of the impedance contrast $\delta = \eta_1/\eta_{air}$ where η_1 is the characteristic impedance of the material surrounding the tunnel and η_{air} represents the air in the tunnel. First $Z = \eta_{air}^2/\eta_1$ and thus

$$|\rho|^2_{max} = \left| \frac{\eta_{air}^2 - \eta_1^2}{\eta_{air}^2 + \eta_1^2} \right|^2 = \left| \frac{1 - \delta^2}{1 + \delta^2} \right|^2 \quad . \tag{3}$$

In Table 3 we have tabulated values of δ for both electromagnetic and compressional seismic waves and a variety of geological materials in which one might find tunnels. At once we see that the impedance contrast for EM waves $\delta_i < 1$ while for P waves $\delta_j \sim 10^4$. Thus impedance contrast is much more strongly influenced by the type of wave used than by the type of geological material in which one finds the tunnel. Figure 8 illustrated the consequences of the vast difference in δ between EM and P waves as illustrated in terms of the power reflection coefficient $|\rho|^2$. For P waves $|\rho|^2$ is unity regardless of the

geologic material while for EM waves $|\rho|^2$ lies in the range 0.5 to 0.9. Since the impedance contrast plays an analogous role in more sophisticated scattering models, we may conclude that for P waves a tunnel will at best always be a very highly reflective scattering object regardless of the surrounding material. For EM waves we may expect a tunnel to be at best somewhat less reflective, depending on the surrounding material, yet still rather high. The words "at best" above refer to the fact that for tunnel widths small compared to the probing wavelength or close to integer multiples of $\lambda_{air}/2$, $|\rho|$ is reduced as illustrated in Figs. 5 and 6.

In terms of attempts to hide a tunnel it is conceivable that in the case of EM waves a tunnel could be at least partially disguised by filling it with material such that the contrast with the surrounding material would be less, $\delta \to 1$. For example, back-filling a tunnel with waste could be a rather effective disguise with regard to EM waves. However, for seismic P waves even relatively small amounts of air remaining in the backfill material would leave the tunnel as a high contrast scattering object. By the same token, as discussed in Section II above, P waves suffer more scattering from geological inhomogeneities than do EM waves.

TABLE 3

Characteristic Impedance Ranges for Electromagnetic and Compressional Seismic Waves in a Variety of Geological Materials

PARAMETER	GRANITES	SALT	SANDSTONES	LIMESTONES	CLAYS OR SHALES
Electromagnetic Waves					
Relative Dialectric Constant,* ε_r	2.8 - 19	~ 5.6	4.7 - 12	7.3 - 7.9	7 - 43
Characteristic Impedance, η_i	220 - 86	~ 160	170 - 110	140 - 130	140 - 58
Impedance Contrast, δ_i	.60 - .23	~ .42	.46 - .29	.37 - .34	.37 - .15
Compressional Seismic Waves					
Seismic Wave Velocity,** c_p in m/s	$(4.6\text{-}7.0)\times10^3$	$(4.4\text{-}4.9)\times10^3$	$(1.9\text{-}5.4)\times10^3$	$(3.5\text{-}7.0)\times10^3$	$(1.5\text{-}4.2)\times10^3$
Density,** ρ in kg/m^3	$(2.5\text{-}2.8)\times10^3$	$(2.0\text{-}2.2)\times10^3$	$(1.6\text{-}2.8)\times10^3$	$(1.7\text{-}2.9)\times10^3$	$(1.6\text{-}3.2)\times10^3$
Characteristic Impedance, η_j	$(12\text{-}20)\times10^6$	$(8.8\text{-}11)\times10^6$	$(3.0\text{-}15)\times10^6$	$(6.0\text{-}20)\times10^5$	$(2.4\text{-}13)\times10^6$
Impedance Contrast, δ_j	$(2.8\text{-}4.7)\times10^4$	$(2.1\text{-}2.6)\times10^4$	$(7.0\text{-}35)\times10^3$	$(1.4\text{-}4.7)\times10^4$	$(7.5\text{-}30)\times10^3$

* Values of ε_r, as quoted by Telford, et al., (1976, p. 456), were measured mainly as frequencies of 100 kHz and up. The relative permeability μ_r was assumed to be unity.

** Values of c_p and P were taken from Telford, et al., (1976) pages 259 and 26 - 27 respectively.

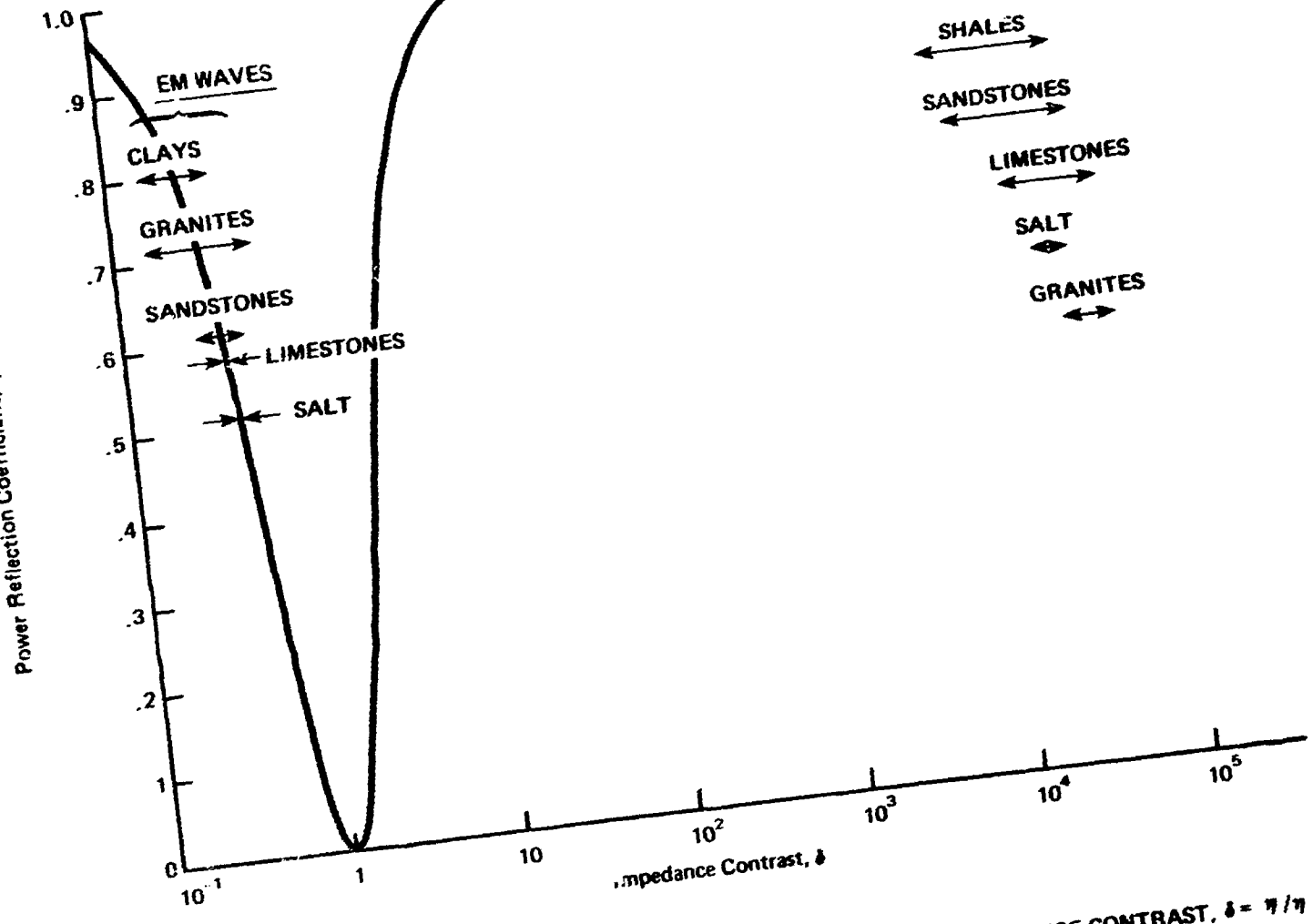

Figure 8 MAXIMUM POWER REFLECTION COEFFICIENT, $|\rho|^2$, AS A FUNCTION OF IMPEDANCE CONTRAST, $\delta = \eta / \eta_{air}$ FOR A SLAB MODEL TUNNEL. THE MAXIMUM OCCURS FOR TUNNEL WIDTHS EQUAL TO $\lambda_{air}/4, 3\lambda_{air}/4, 5\lambda_{air}/4$, etc. ALSO SHOWN ON THE FIGURE ARE THE RANGES OF δ EXPECTED FOR ELECTROMAGNETIC AND COMPRESSIONAL SEISMIC WAVES IN A VARIETY OF GEOLOGICAL MATERIALS - see Table III.

2. Scattering Calculations for Cylindrical Objects

Among the simple geometrical shapes, tunnels correspond most closely to cylinders, and wave scattering from cylinders has been extensively studied, both theoretically and experimentally; e.g., see Ruck, et al, (1970), King and Wu (1959) or Bowman, Senior and Uslenghi (eds., 1969) for general treatments. Most treatments of scattering from cylinders involve a cylinder, surrounded by air, which is either a perfectly conducting rod or tube or a dielectric rod or tube: Barrick (1968), Burke (1964), Bussey and Richmond (1975), Konyounijian, Peters and Thomas (1963), Lytle (1971), Lytle and Lager (1976), Morse (1964), Tsandoulas (1968), and Wait (1955). While these treatments can provide helpful guidance, they are not specific to the situation at hand. For example, the intrinsic impedance of a tunnel is higher than that of the surrounding medium rather than lower as would be the case for a dielectric cylinder surrounded by air.

However, Howard (1972) does treat the case of a subterranean cylindrical (circular) inhomogeneity. He uses a mode matching method to find the solution for the anomalous fields caused by the buried cylinder in an otherwise homogeneous lower half-space. A numerical calculation for a buried conductor is presented in which Howard's solution, truncated to five modes, is found to be virtually identical to a solution by "Wait's method" (Wait, 1972). Further pursuit of Howard's work could well be fruitful if information beyond the simple diffraction model discussed below is needed.

Lytle and his colleagues have done considerable work on both the theoretical and experimental sides of tunnel detection, in particular

using HF and VHF radio waves propagated between boreholes as illustrated in Fig. 7, Lytle (1971) and Lytle and Lager (1976) and Lytle, et al, (1976 and 1977). This work has included calculation of wave diffractions by circular and realistically shaped tunnels in order to simulate the data to be collected in experiments. Their emphasis at the time of the Lytle, et al, (1977) report was on wave amplitude and using classic back projection techniques to map out the area between the borehole sensors on the basis of data collected along the borehole. Summaries of their work are contained in workshop reports by Stanford Research Institute (1976a and b, and 1977).

Moment methods (Harrington, 1968) provide a powerful means of studying scattering problems numerically. In fact the third chapter of Harrington's book is largely devoted to scattering from cylinders. The beauty of the moment method is that inhomogeneities and unusual geometries can be handled. Peters in (Stanford Research Institute, 1977) uses moment methods to calculate the scattered field from a square tunnel.

C. Diffraction Model for Scattering by a Tunnel

1. High Contrast Tunnel as a Diffracting Screen

From Fig. 8 above it is evident that tunnels will present a very high contrast (highly reflecting) target to P waves and a high contrast target to EM waves in most media. Hence in this approximate model we will view the tunnel as a plane diffracting screen, i.e., as a perfectly conducting (EM waves) or perfectly rigid (P waves) and hence opaque strip. The idea is illustrated in Fig. 9. Further, in Table 2 above we

note that for EM and P wavelengths which are near or shorter than the resonant wavelength for the tunnel (radiation wavelength = tunnel circumference) absorption in the medium surrounding the tunnel plays an important role. Because absorption grows exponentially with distance, ray paths which deviate markedly from the most direct route between source and sensor quickly become less important as r_t and r_r increase (see Fig. 9).

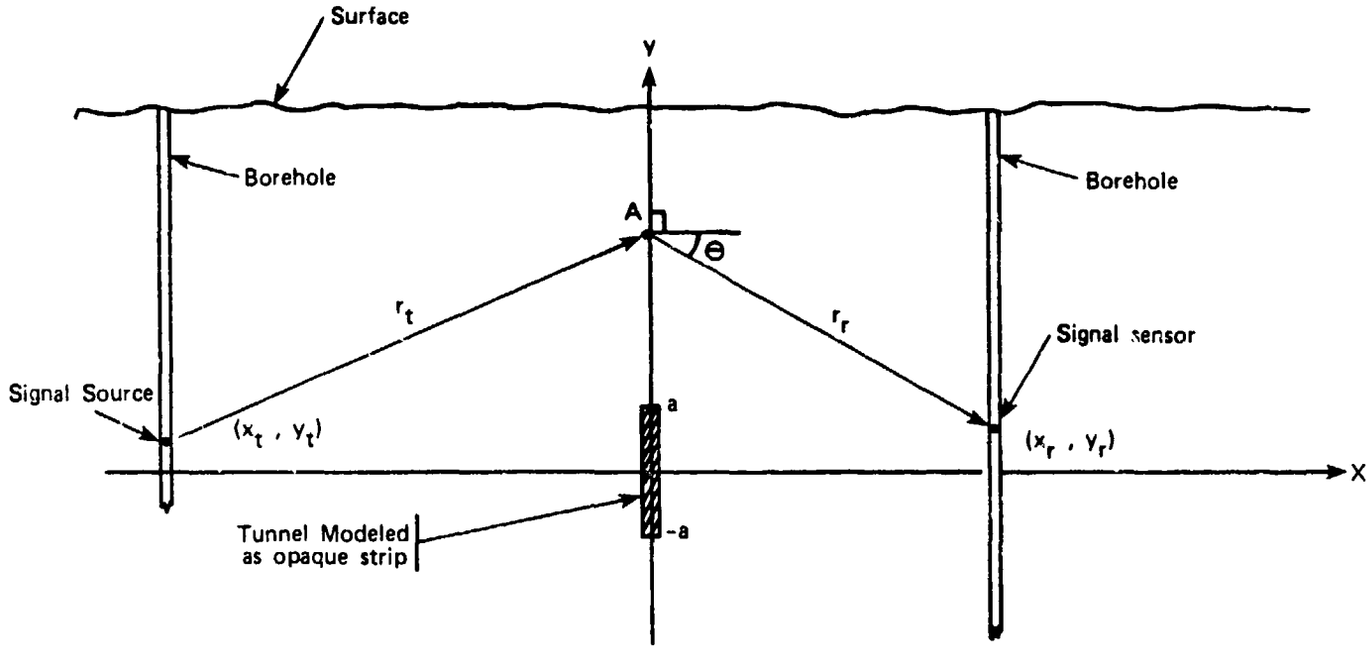

Figure 9. Two dimensional diffraction model with tunnel approximated as opaque strip. Seismic or electromagnetic waves are emitted by a source, diffracted by the tunnel (opaque strip) and received by a sensor or group of sensors on the other side of the tunnel. Since we are interested mainly in variations along the y direction, we use a two dimensional model where the signal source and sensor as well as the tunnel are assumed to extend to large distances perpendicular to the (x,y) plane; i.e. the source is a line source perpendicular to the (x,y) plane, the tunnel a strip perpendicular to the (x,y) plane and the sensor a line sensor in the y direction.

2. Formulation of the Diffraction Model with Attenuation

To calculate the field at the sensor we use scalar diffraction theory with the addition of an attenuation term. Using the Huygens-Fresnel principle one simply integrates along the y-axis summing the contributions of rays passing between source and sensor via points A as shown in Fig. 9. Since we are principally interested in variations along the y direction (along the borehole) and since it simplifies the mathematics, we consider the two dimensional case where a line source is diffracted by an opaque strip both of infinite extent along the z direction [perpendicular to the (x, y) plane]. Thus we do not consider variations along the z direction. Adapting the Rayleigh-Sommerfeld diffraction formula (see, for example, Goodman, 1968, Ch. 3) to the two dimensional case and inserting an attenuation factor, we have

$$U(x_r, y_r) = (B/j\lambda) \int_{-\infty}^{\infty} (r_t r_r)^{-1} \exp\left[(-\alpha + jk)(r_t + r_r)\right] \cos\Theta \, dy \qquad (4)$$

where U is the complex scaler field observed at (x_r, y_r), B the source amplitude, λ the wavelength in the medium, $j = \sqrt{-1}$, α the attenuation factor in nepers m^{-1}, $k = (2\pi/\lambda)$, $\cos\Theta$ (the obliquity factor) $= (x_r/r_r)$ and the other items are given in Fig. 9. This integral was decomposed into real and imaginary parts and each part evaluated numerically using series summations to approximate integrals. The terms in these sums corresponded sequentially to large and larger values of

thus making sequentially later terms generally smaller due to attenuation and geometry. Each integral was thus evaluated over y values corresponding to at least the first four Fresnel zones. Terms corresponding to larger values of y were added until succeeding increments added less than 0.5% to the total intensity of the field $|U|^2$.

3. Accuracy of the Diffraction Model

Since this diffraction model corresponds only approximately with physical reality, it is important to discuss the principal sources of error and how important each is likely to be. To begin with we have assumed the tunnel to be a thin opaque screen with sharp edge whereas the real tunnel is cylindrical, does transmit some energy through it and has rough edges. Since it is beyond the scope of this report to compare scattering by a thin screen with that of a rough cylinder, we argue that the principal physical effect of either is to inhibit radiation from propagating between source and sensor and in this respect the thin screen approximation appears intuitively to be reasonably sound. An estimate of just how opaque a tunnel is likely to be can be made by considering Figs. 5, 6 and 8. From Fig. 8 we find that maximum power reflection coefficients $|\rho|^2$ at a rock-air interface vary from about 0.5 to 0.8 for EM waves and are close to 1 for seismic P waves. Further from Figs. 5 and 6 we note that for a slab model tunnel (see Fig. 4) $|\rho|^2$ varies considerably depending on tunnel width and wave frequency though usually being near the maximum value. Because waves striking a cylindrical tunnel are not normally incident as with a slab and because the cylindrical geometry would tend to scatter waves in all directions, we would expect that considerably

less than half, probably less than a tenth of the incident EM power would be transmitted directly through an air-filled tunnel. For seismic P waves $|\rho|^2$ is usually near one and very little P wave power would be transmitted. Thus the assumption of an opaque tunnel is reasonably good for EM waves and quite good for P waves. However, for particular geometries and wave frequencies significant amounts of power can be transmitted directly through a tunnel and this transmitted energy will fill in the shadow of the tunnel shown in Figs. 10-17, thus making the signature of the tunnel more difficult to detect.

The Huygens-Fresnel principle which leads to Eq. (4) is quite accurate provided $kx_t \gg 1$, $kx_r \gg 1$ and $2ka \gg 1$ (Silver, 1962). At the higher frequencies considered here (> 2kHz for P waves and > 120 MHz for EM waves) these conditions are fulfilled. However, at the lower frequencies (< 500 Hz for P waves and < 30 MHz for EM waves) the inequalities above are not rigorously fulfilled and the resulting calculations can only be considered as roughly correct. Since the diffraction model considered here is an approximation in any case, the fact that the wavelength λ is of the order of the tunnel size at the lower frequencies is not a serious drawback.

In the case of EM waves, polarization comes into play; yet we are using a scalar diffraction theory which ignores polarization. The principal effect of wave polarization would appear to be in the boundary conditions. Since waves with the $\vec{E}$ field polarized along the tunnel length (along the z-axis) would be more strongly reflected from a

cylindrical tunnel, they would correspond more closely to our opaque screen approximation and thus presumably agree more closely with the results reported below. Similarly waves with $\vec{E}$ polarized perpendicular to the tunnel would presumably correspond less well to the results given below.

D. Diffraction Model Results

1. Stationary Source and Multiple Sensor Locations

In this section we consider a stationary original source located at varying x_t, but with $y_t = 0$ and multiple sensors or a movable sensor located at varying (x_r, y_r); see Fig. 9. Although we later consider the case where both source and sensor move together such that $y_t = y_r$, it may well be that the difficulty of moving both source and receiver simultaneously will make the stationary source case, which we consider here, more operationally feasable. We first consider EM waves and subsequently compressional seismic (P) waves. The physical properties of the propagating medium are those for solid granite as shown in Table 2.

a. Electromagnetic Waves

As an illustrative example, we consider a case where the source is located at the same depth as the tunnel ($y_t = 0$ in Fig. 9) and some 20 m from the tunnel center ($x_t = -20$m). The sensors or movable sensor are located much closer to the tunnel ($x_r = 5$m). Letting $B = 1$ in Eq. (4), the received signal intensity $|U|^2$ in Eq. (4) and phase are calculated for varying locations along the borehole (y_r varies). Since the source is placed at the same level as the tunnel, only results for $y_r > 0$ are shown--the results for negative y_r being symmetric.

In Fig. 10 we consider diffraction model results for 60 MHz propagating in granite with and without a 2 m diameter tunnel present (a = 1 in Fig. 9). The tunnel reduces the expected intensity by as much as a factor 3.3 (5.2 db). The phase contrast between the two cases is as much as 0.55 radians (31^{o}). The maximum intensity anomaly occurs some 1.6 m both above and below the tunnel center level whereas the maximum phase anomaly occurs at one location directly behind the tunnel. The contrast between the rather smooth nature of the curves without the tunnel present and the more rapidly and characteristically varying curves with the tunnel present suggests that a spatial matched filter might prove effective in detecting the tunnel. We discuss this possiblity below.

In Fig. 11 intensity and phase for three different frequencies are shown. For propagation at 30, 60 and 120 MH_2 (in granite) the wavelengths of the probing waves are 5.7, 2.9 and 1.5 m respectively or $ka = 1.1$, 2.1 and 4.2 . The quantity ka (where the wave number $k = 2\pi/\lambda$ and a is the tunnel radius) is well known as a characteristic parameter in scattering problems (e.g., see Jenkins and White, 1976, Ch. 18). In this case it turns out to be the tunnel circumference divided by the probing wavelength λ . The larger ka , the more pronounced the oscillations shown in Fig. 11 and the shorter the length scale (in y_r) of the oscillations. Although the attenuation (α) does have a significant influence on the shape of the intensity and phase curves (Fig. 12), both these curves remain rather similar in shape for changes in α and λ which retain a constant value of ka.

The intensity level varies quite dramatically with frequency. For the geometry of Fig. 11 we find that maximum intensities drop rapidly with increasing frequency because absorption increases with frequency in granite. The maximum intensities at 60 and 120 MHz are 16 and 60 db smaller than the maximum intensity at 30 MHz. We also need to consider the overall signal loss between source and receiver. For 30, 60 and 120 MHz the source to sensor signal power loss at the location (y_r, of maximum intensity is 78, 94 and 139 db respectively. It is quite clear from this chat although the tunnel signature is more prominent at higher frequencies, there is also a very serious penalty in terms of signal strength at higher frequencies. Hence one is faced with the common engineering problem of juggling range, frequency, etc., to obtain an optimal system in terms of low false alarm rate and high detection probability. Here the problem is complicated by geological inhomogeneities masquerading as tunnels (see Chapter II).

Obviously the degree of absorption in the propagation medium has a very strong effect on received signal intensity. But how does it affect the form of the tunnel signature? To answer this question Fig. 12 compares tunnel signatures for two cases: one a low absorption case (α = 0.5 db/m) and the other with absorption appropriate to granite as shown in Table 2. Aside from absorption, the cases are identical. Very little change occurs in the phase signature. However, the intensity signature is significantly more pronounced when the absorption is low. Thus any detection scheme which depends on the form of the tunnel signature must also take the absorption characteristics of the propagation medium into account in estimating the expected tunnel signature.

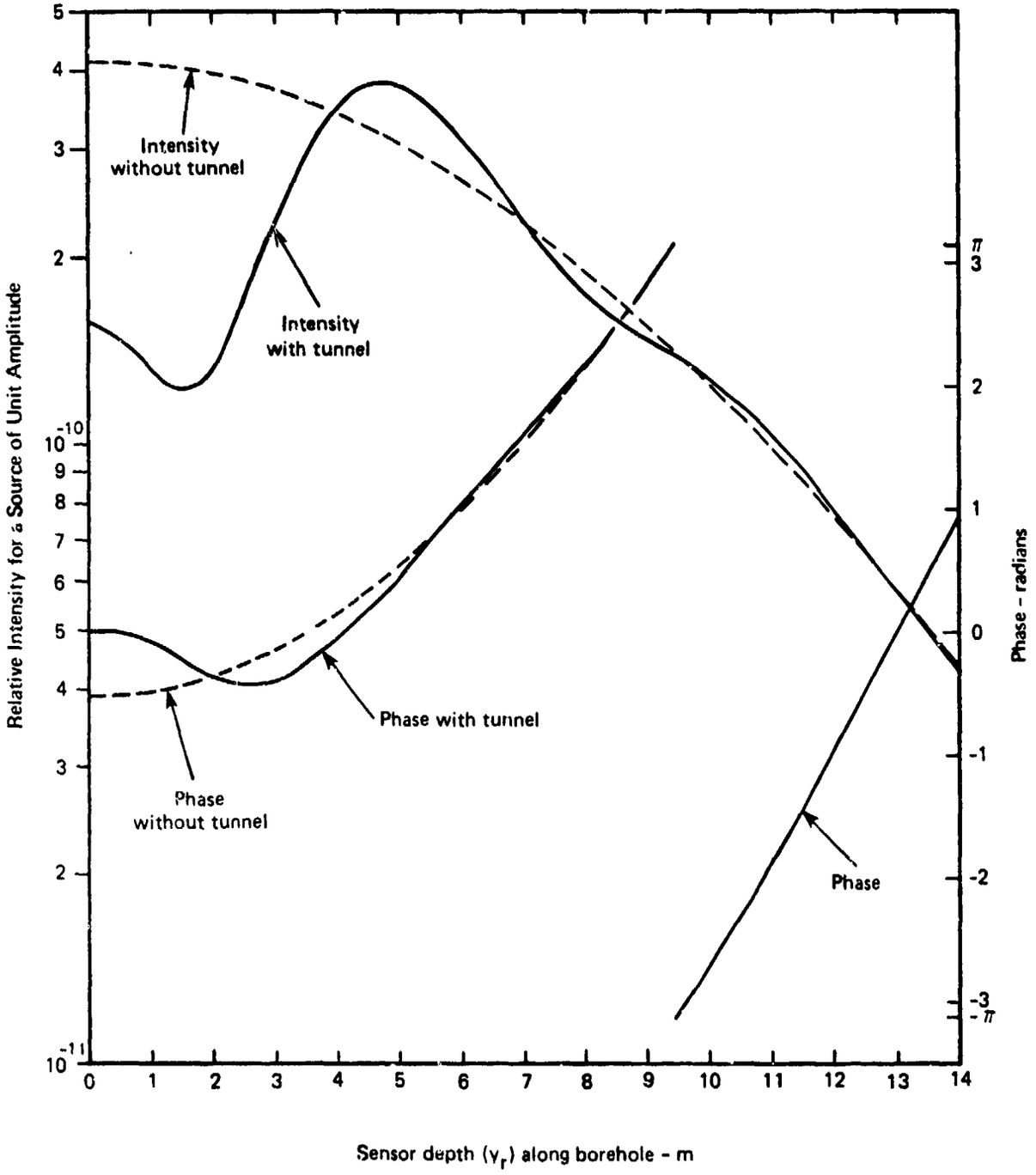

Figure 10. Relative intensity and phase of received EM signal as a function of sensor depth along borehole. The geometrical parameters (see Figure 9) are: $x_t = -20$ m, $y_t = 0$ m & $x_r = 5$ m. The propagating medium is granite with $\epsilon_{rel} = 2.9$ and power attenuation = 2.2 db m^{-1} for a frequency of 60 MHz. Signal phase has been normalized such that it is 0 with tunnel present at $y_r = 0$. Sensor depth is relative to depth of tunnel which has a diameter of 2 m.

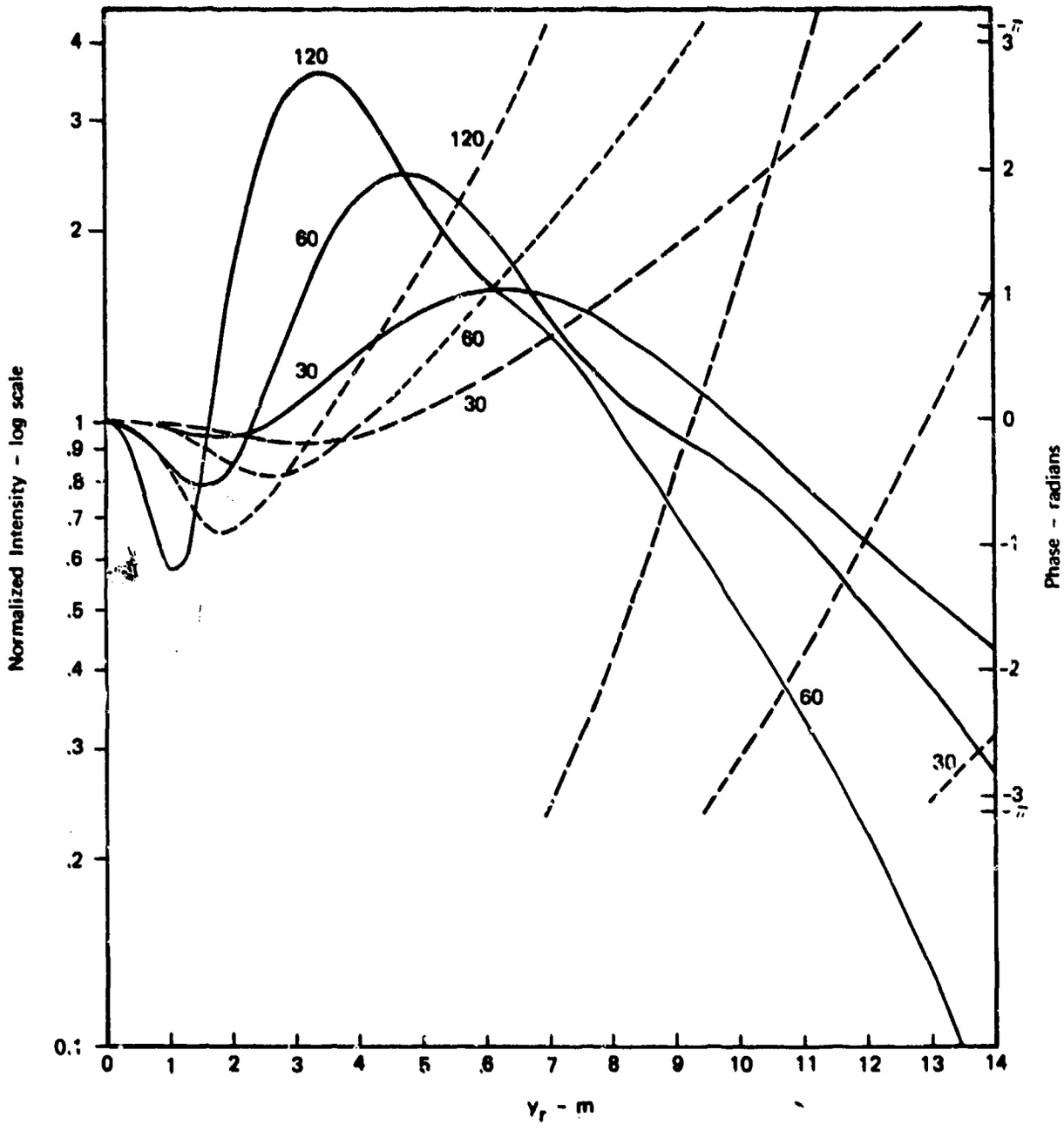

Figure 11. Normalized intensity (____line) and phase (– – –line) of received EM signal as a function of sensor depth along borehole (y_r). The model results for these frequencies corresponding to ka = 1.1, 2.1 & 4.2 are compared using propagation parameters for granite, see Table 2. The geometrical parameters are the same as for Figure 10. Signal intensity has been normalized such that it is zero as y_r = 0. The actual intensities at 30, 60 and 120 MHz have been multiplied by factors of 1.03×10^{8}, 6.37×10^{9} and 2.54×10^{14} to normalize them to unity for comparison.

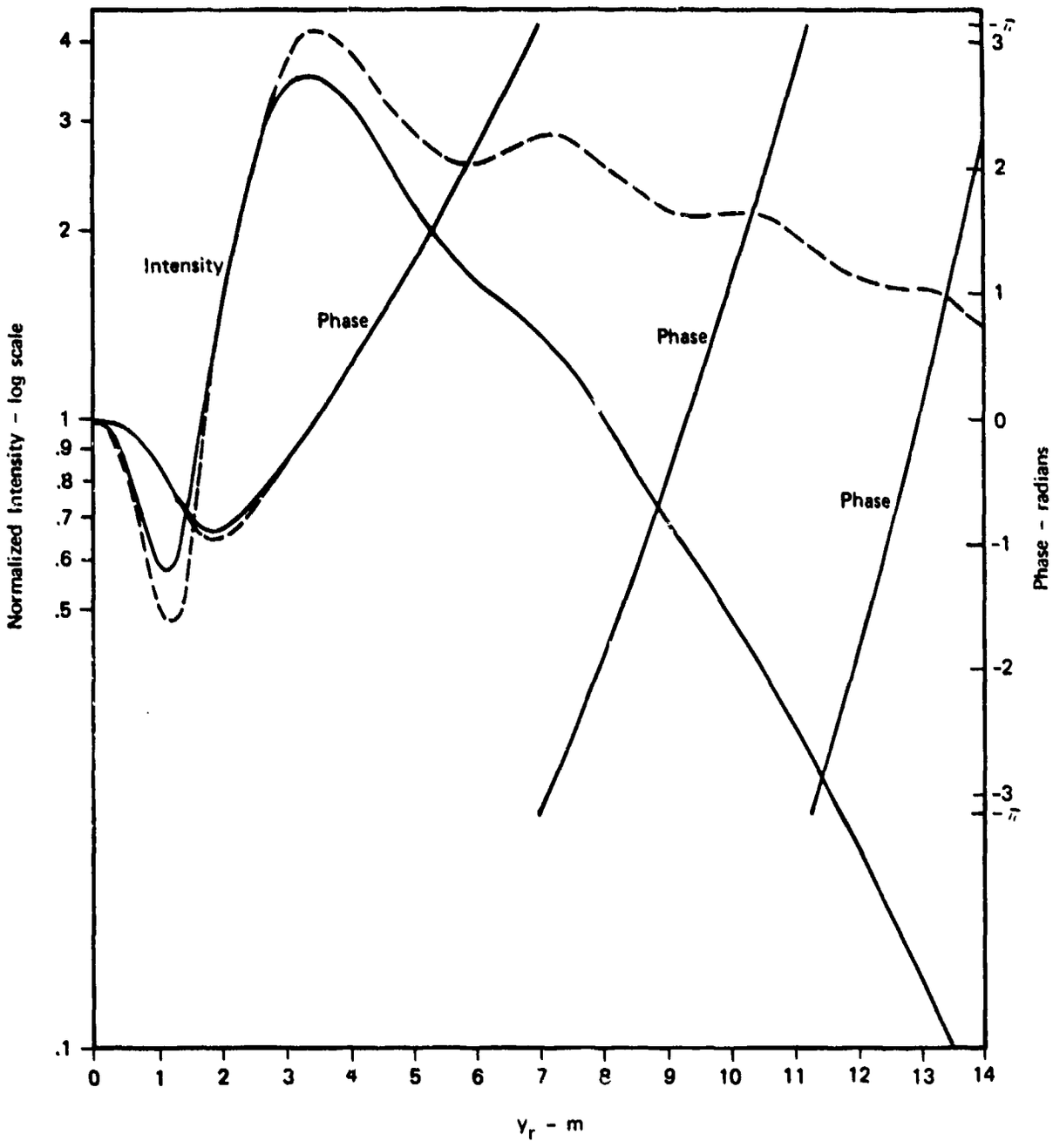

Figure 12. Normalized intensity and phase of received EM signal as a function of sensor depth along borehole (y_r). Model results are compared at 120 MHz for a case with very low attenuation (α = 0.5 db/m, dashed line) and a case with absorption appropriate to solid granite (α = 4.1 db/m, solid line). Geometrical parameters are the same as Figure 10. Signal phase has been normalized to zero at y_t = 0. The actual signal intensities have been multiplied by 2.2×10^5 for the low absorption case and 2.6×10^{14} in the granite absorption case to normalize them to unity at y_r = 0. Note the more pronounced tunnel signature in the low absorption case (dashed line).

The diffraction model results shown thus far have been for a tunnel much closer to the sensor borehole than the source borehole. In Fig. 13 we find that the tunnel signature becomes less pronounced as the distance between tunnel and sensor increases. When the tunnel is close to the sensor the maximum intensity occurs away from the x-axis (see Fig. 9) although a local maximum does occur on the x-axis ($y_r = 0$) . When the tunnel is at a sufficiently large distance from the sensor the overall intensity maximum occurs on the x-axis as it does when no tunnel is present. In the figure we consider a typical case in which the source and sensor boreholes in Figs. 7 and 9 are 25 m apart. Solid granite is the propagating medium for 60 MHz electromagnetic waves. Figure 13 gives signal signatures for cases with no tunnel present and 1 m radius tunnels at 5, 12.5 and 20 m from the sensor borehole. Even at a signal to noise/clutter ratio of unity it appears that the tunnel could be detected if it were closer to the sensor borehole than the source borehole. Detection appears unlikely for the tunnel 20 m from the sensor borehole unless there were some reliable way to establish the signal level one would expect in the absence of a tunnel. Given the inhomogeneous nature of the propagation medium and difficulties with calibration, it appears likely that one would be forced to rely only on the signature shape. In this case tunnels near the source would be difficult to detect. Schemes to get around the necessity of having the tunnel near the sensor are discussed in section F below, e.g., swapping source and sensor boreholes.

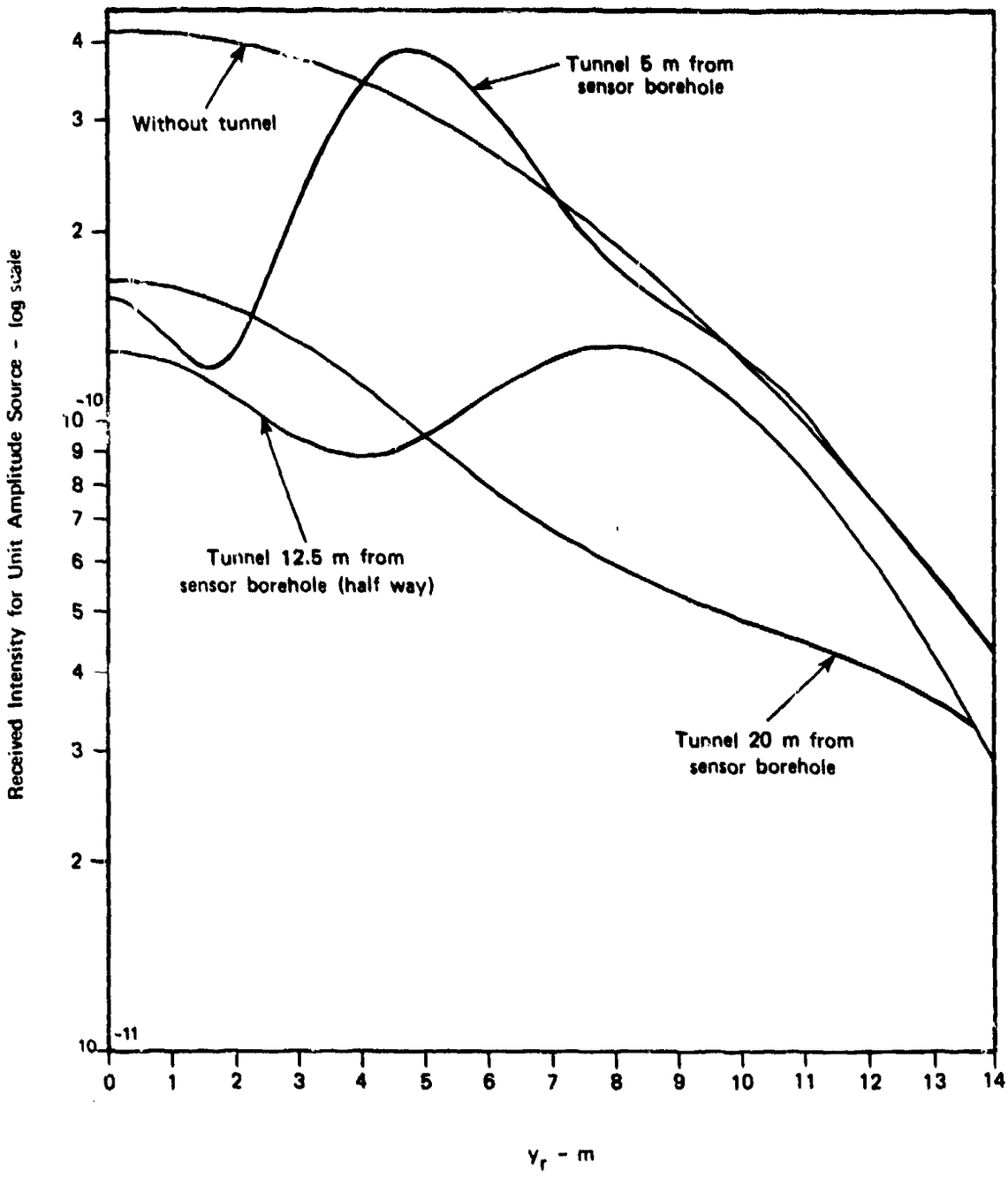

Figure 13a. Received intensity of EM signal as a function of sensor depth along borehole (y_r). Received signal is compared for no tunnel and a 1 m radius tunnel at three distances from sensor borehole with source and sensor boreholes 25 m apart. Propagation constants are for solid granite and 60 MHz EM waves. Note how tunnel signature fades as tunnel is located at increasing distances for sensor.

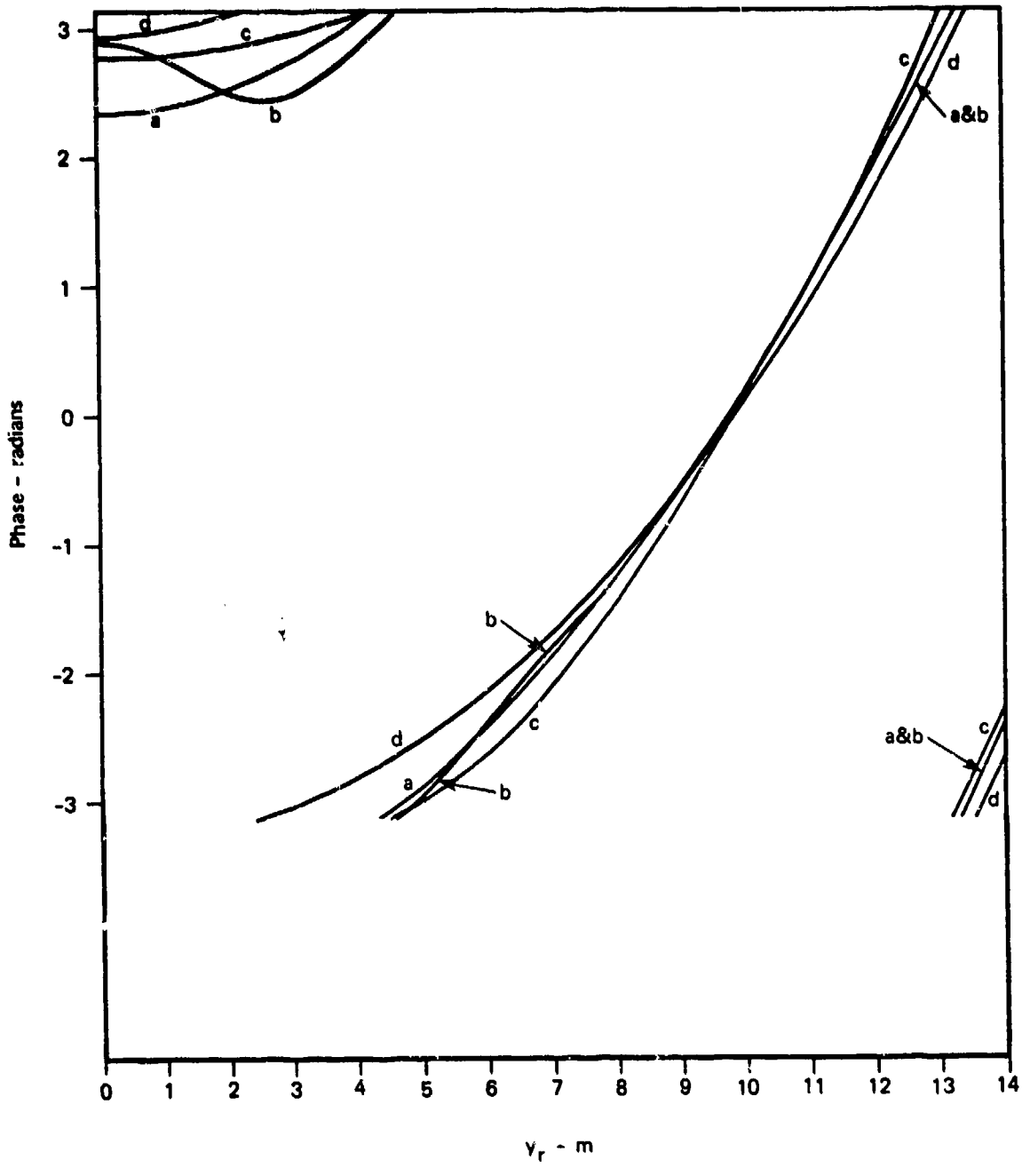

Figure 13b. Phase of 60 MHz received signal as a function of sensor depth along borehole (y_r). Signal phase is compared for four cases: (a) tunnel absent, (b) tunnel 5 m from sensor (borehole), (c) tunnel 12.5 m from sensor (half way) and (d) tunnel 20 m from sensor. In all cases the sensor and source boreholes are 25 m apart and propagation constants are for solid granite.

It is interesting to note that there is a very pronounced phase signature (b) in Fig. 13b when the tunnel is 5 m from the sensor borehole. If reliable phase measurements could be made, the phase signature might in fact be more detectable than the intensity signature. This of course depends on the nature of the apparatus used.

b. Seismic Waves

Compressional seismic (P) waves behave much the same as EM waves (having the same value of k in the medium) considered above with two important differences. First the P waves suffer much less absorption (Table 2), and second the P waves have much greater reflection coefficients at typical interfaces (Figs. 6 and 8).

In Fig. 14 we compare the EM and P wave intensity and phase signatures of a 1 m radius tunnel. The geometrical parameters (see Fig. 9) are the same as for Fig. 10: source borehole 20 m from tunnel and sensor borehole 5 m from tunnel. The wave transmitter is stationary at the tunnel depth ($y_t = 0$) and the receiver is moved vertically. The most obvious difference between the EM and P wave signatures is the intensity level. The P wave signal suffers a transmission loss about 50 db smaller than the EM signal. The lower attenuation for P waves results in a somewhat more prominent intensity signature than for EM waves. However, the phase signatures are very similar.

Aside from the aforementioned transmission loss differences and some secondary changes in intensity signatures, the main

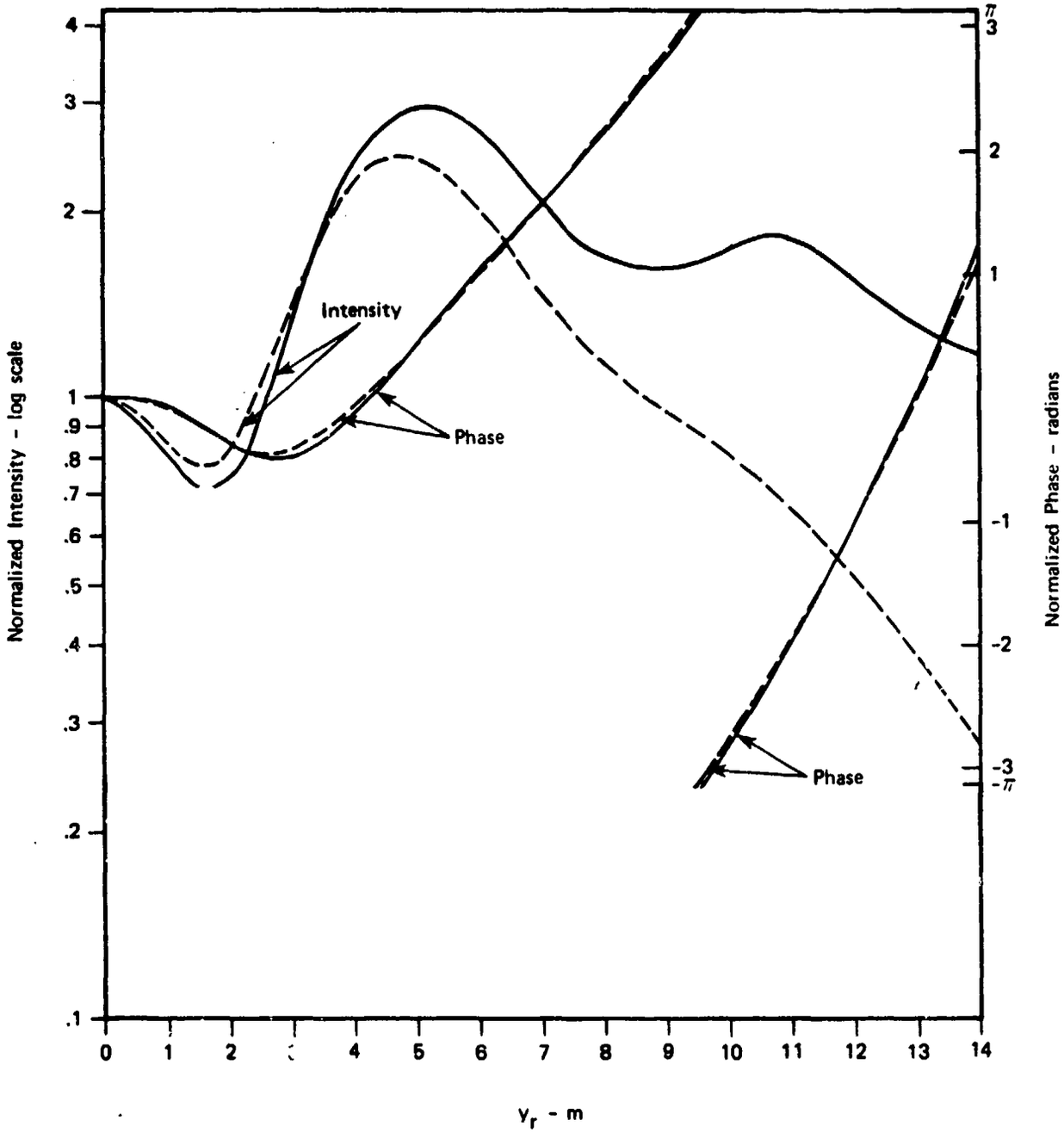

Figure 14. Comparison of tunnel signatures (intensity & phases) for 1.7 kHz compressional seismic (P) waves (_____) and 60 MHz EM waves (– – – – –). The geometry (Figure 9) is the same as for Figure 10: 1 m radius tunnel, 5 m from sensor and 20 m from source. The propagation medium is solid granite (see Table II). The EM wave intensity has been multiplied by 6.4×10^9 and the seismic wave intensity by 10^5 to normalize them to unity at $y_r = 0$. The wavenumber in the medium k is the same, namely 2.14, for both the EM and P waves.

points illustrated in Figs. 10-13 for EM waves apply to P waves having the same wave number k. As discussed in Chapter II, for EM waves in most earth materials $k = 2\pi f\sqrt{\varepsilon_r/c_o}$ where f is wave frequency (Hz), ε_r relative permittivity and c_o the speed of light in a vacuum, while for P waves $k = 2\pi f/c_p = (2\pi f\sqrt{\rho})/\sqrt{K + (4/3)\mu}$ where c_p is phase velocity for P waves (Table 1), ρ mass density, K bulk modulus and μ rigidity or shear modulus.

One obvious consequence of the lower attenuation experienced by P-waves is that one can put boreholes further apart for the same system loss. We have illustrated this capability in Fig. 15. The source and sensor boreholes are 50 m apart with the 2 m diameter tunnel 10 m from the sensor borehole. This is twice the 25 m borehole separation of Figs. 10-14. For the 1700 H_2 P-wave we find the propagation loss to be about 63 db and we note that the characteristic tunnel signature is quite prominent. In these circumstances the 60 MHz EM signal propagating in granite, which we have considered previously, has a propagation loss of some 161 db--nearly 100 db higher than the P-wave loss. In addition we see that the characteristic tunnel signature is more pronounced in the P-wave case.

c. Source Not at Tunnel Level

Since the tunnel location and even existence of a tunnel is unknown, the source may not in fact be at the tunnel level as assumed in Figs. 10-15. Of course one would make observations with the source at various levels. However, it is of interest to know how the tunnel signature is distorted when the signal source is not at the tunnel level.

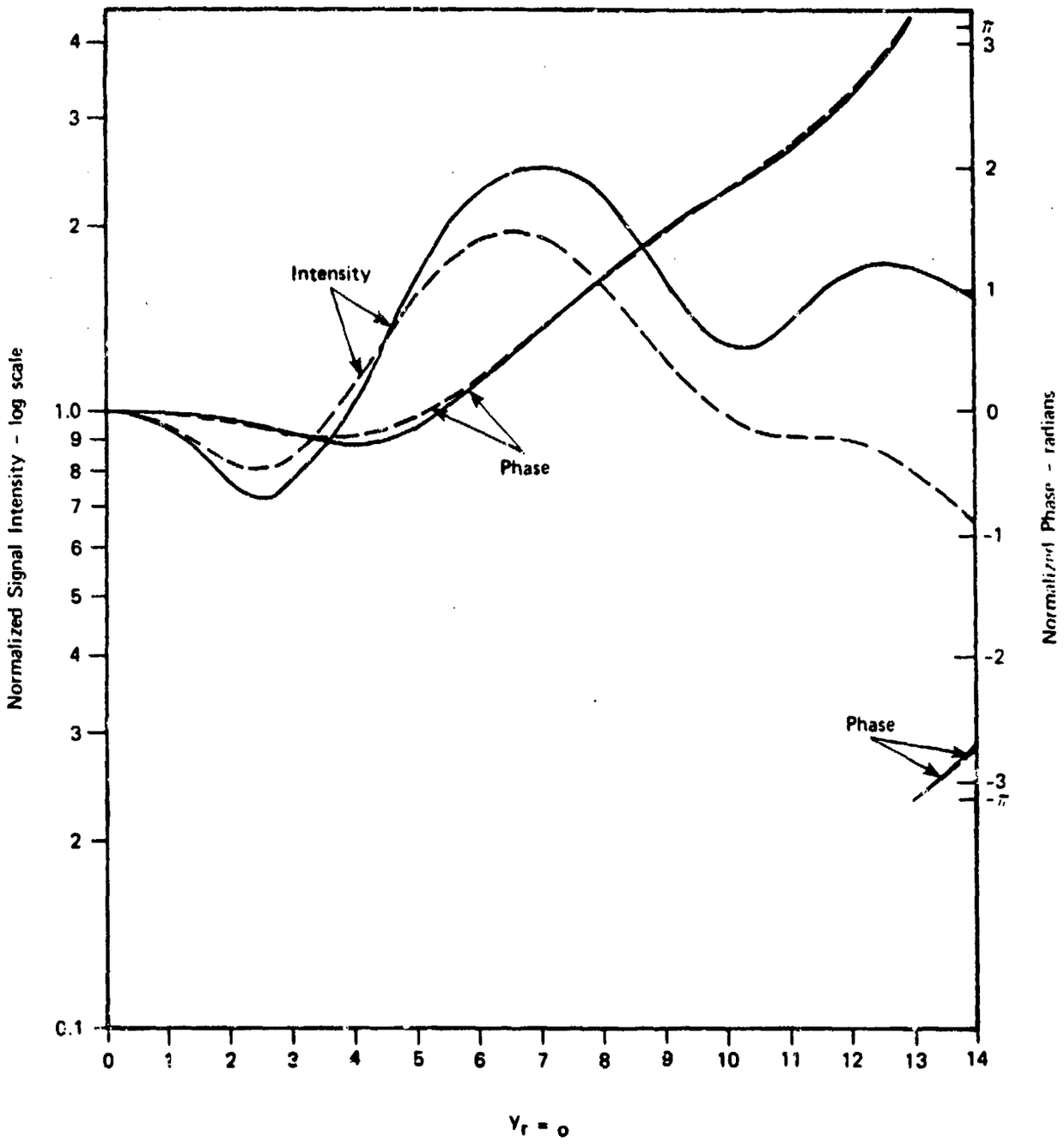

Figure 15. Comparison of tunnel signatures for compressional seismic (P) waves (solid line) and EM waves (dashed line) with source and sensor separated by 50 m. The 2 m diameter tunnel is located 10 m from the sensor borehole. In the granite propagating medium k = 2.14 for both P and EM waves. The EM wave intensity has been multiplied by 1.2×10^{16} and the P wave intensity by 3.3×10^{6} to normalize them to unity at $y_r = 0$. (y_r is depth in the sensor borehole relative to the tunnel level.) i.e. $y_t = 0$ in Figure 9. In Figure 16 we show model results for a case where source and sensor boreholes are 25 m apart and the tunnel is 5 m from the sensor borehole. However, the source is not at tunnel level ($y_r \neq 0$) as in Figure 10, but rather displaced 5 m below tunnel level along the source borehole.

It is clear from Fig. 16 that the offset of the source introduces a major asymmetry in the tunnel signature. First the phase signature of the tunnel shadow is shifted from $y_r \approx 0$ to higher values of y_r. Further the diffraction peak above the tunnel level is significantly enhanced while the peak below the tunnel level is reduced. Comparing these results to Fig. 10 we see that displacing the source from tunnel level significantly distorts the intensity signature while the phase signature is more displaced than distorted.

2. Source and Sensor at Same Vertical Level

Although resulting in more complex apparatus and operational procedures, it is clearly possible to vary the vertical level of both the source and sensor in Fig. 9 or to have multiple sensors in both source and sensor boreholes. Observations in this mode hold attenuation losses to a minimum since source and sensor are always at minimum separation. They also have the advantage that one expects a constant signal level if no tunnel or other propagation disturbance is present. In Fig. 17 we show model results for a 60 MHz EM wave propagating in granite. The source and sensor boreholes are 25 m apart with the tunnel 5 m from the sensor borehole. This allows direct comparison with Fig. 10 which has the same parameters, but a fixed source. The tunnel signature for intensity is somewhat more prominent in Fig. 17 than in Fig. 10--the peak (P) to valley (V) ratio being 4.5 in the latter case and 3.2 in the former. When the tunnel is nearer the source than the sensor, the tunnel signature is spread over larger values of y_r (see Fig. 13). In this situation the $y_t = y_r$ observation mode would be of more help since it would limit attenuation

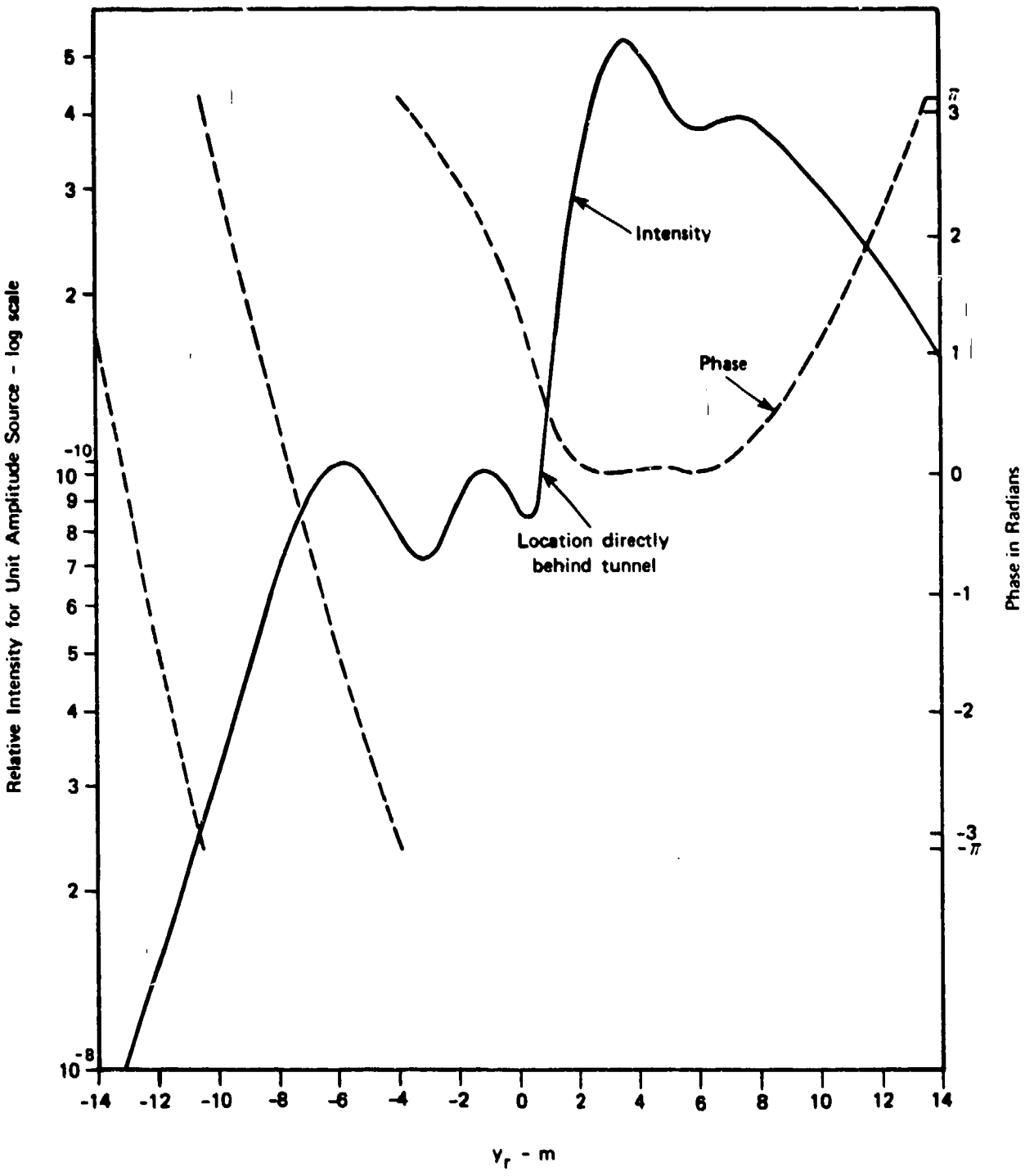

Figure 16. Relative intensity and phase of received EM signal as functions of sensor depth along borehole (y_r). The source and sensor boreholes are 25 m apart with the tunnel 5 m from the sensor borehole. The source is not at tunnel level, but rather 5 m (y_t = -5 in Figure 9) below tunnel level. Propagation parameters are for 60 MHz, EM waves in solid granite. Note how the intensity signature is displaced and greatly distorted relative to Figure 10 while the phase signature is more displaced than distorted.

losses at large y_r . We note here that simple geometrical considerations allow one to construct Fig. 17 given Fig. 10 and the observational geometry. However the constructed version would suffer from reduced signal to noise ratio at large y_r .

3. Forward Scatter Enhancement

Since the present scheme involves forward propagation past an object, one might hope to make use of forward scatter enhancement when source and sensor are sufficiently removed from the tunnel. For example in the far zone the scattering width of an infinitely long conducting cylinder shows enhancement along the forward scatter direction as shown in Fig. 18. The large forward scatter enhancements are, however, observed for large values of ka ($=2\pi a/\lambda$) whereas here we consider values of ka near unity where forward scatter enhancement is rather small. One could raise the operating frequency to raise ka and thus presumably create a significant forward scatter enhancement. In the EM wave case attenuation increases rapidly with frequency (Fig. 1) so that use of higher frequencies is very limited. In the seismic P-wave case attenuation does increase with frequency (Table 2), but not as rapidly as with EM waves. So the use of P-waves at higher frequencies to exploit forward scatter enhancement is a possibility. However, one would have to balance any advantages gained by forward scatter enhancement against the loss in signal power caused by larger attenuation losses. We also note that the roughness of the tunnel walls and non-cylindrical shape of real tunnels would reduce the forward scatter enhancement.

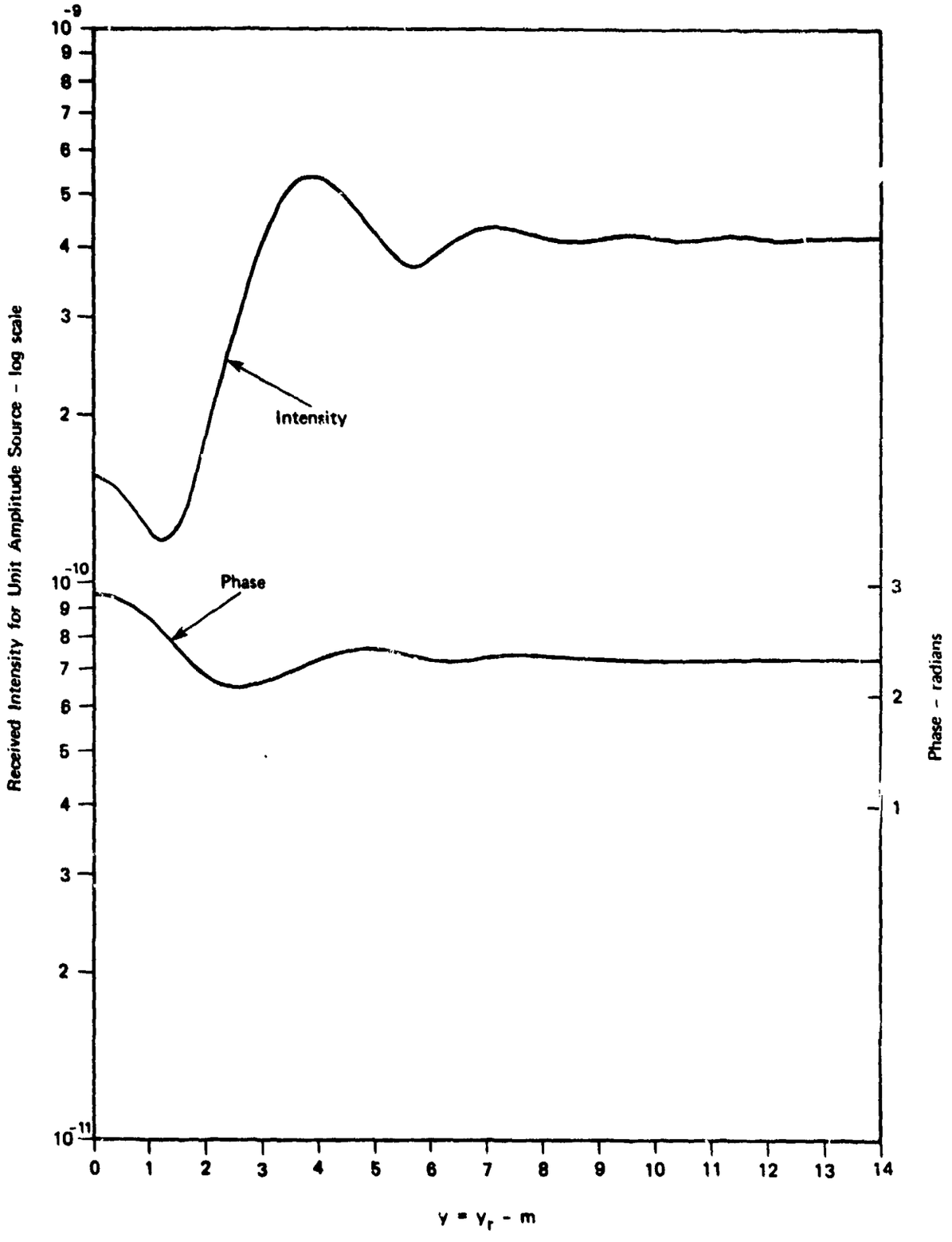

Figure 17. Relative intensity and phase of received EM signal as functions of source and sensor depth ($y_t = y_r$ in Figure 9). These levels are relative to the tunnel level, denoted as zero. The boreholes for source and sensor are 25 m apart with the 2 m diameter tunnel 5 m from the sensor borehole. The 60 MHz EM waves are propagating in granite (Table II). Compare with Figure 10 which has the same parameters, but a fixed source and moveable sensor.

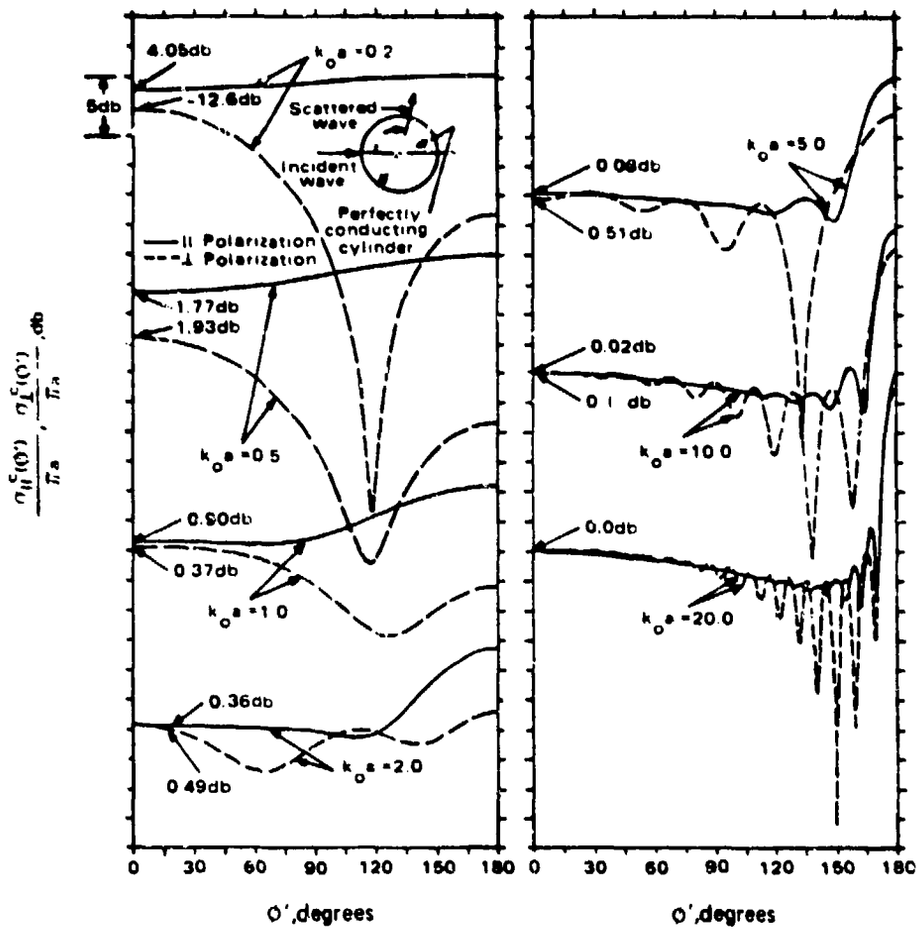

Figure 18. Exact solution for the normalized bistatic scattering widths of an infinitely long, perfectly conducting circular cylinder for various values of $k_o a$ (ka in our notation). These calculations are for an incident plane wave and observer in the far zone. Perpendicular polarization refers to the incident E field being perpendicular to the cylinder's axis. Note that forward scatter enhancement ($\theta' = 180^o$) is a strong function of polarization and $k_o a$ (after Ruck, et al., 1970).

4. Comments & Conclusions

A question which immediately arises is whether EM waves or seismic P-waves are distinctly superior in tunnel detection work. It is clear from our model results above that seismic P-waves suffer much less attenuation during propagation and produce more salient tunnel signatures for a given borehole separation; therefore, instrumentation limitations are important in any overall system evaluation. Suitable measuring apparatus for both EM waves (Lytle, et al., 1976 and 1977) and P-waves (Cratchley, et al., 1976) does indeed exist. However, the maximum signal source power, sensor noise level, ambient noise level, etc., that can be obtained for either case have not been researched in this report. Nevertheless, borehole to borehole measurements have been made using both types of waves (as referenced above). Even given these uncertainties, it appears that seismic P-waves have a significant advantages over EM waves for air filled tunnels, i.e., no conductors (such as rails) in the tunnel.

Analogous to the choice between EM and seismic waves, there is the choice between amplitude and phase measurements or to use both in a vector aproach. Similarly, the choice depends on the measurement apparatus used as well as the particular geological setting and tunnel characteristics. Thus if signal phase (or pulse travel time) can be measured more accurately than can signal amplitude, and/or the phase background fluctuations are small relative to amplitude fluctuations, the signal phase could well provide a more detectable tunnel signature. To the author's knowledge phase measurements have not yet been studied experimentally as a means of tunnel detection.

In assessing the sensor noise level it is important to note that signal propagation from source to sensor via unwanted paths will very likely be the dominant noise source rather than ambient noise. For example reflections from near surface layers or other large scale subterranean discontinuities would propagate significant power from source to sensor as would equipment cables. In radar terminology such unwanted signals are called clutter and the signal tc clutter ratio is the important factor replacing the signal to noise ratio.

In field observations one could use either continuous waves (CW) cr pulse type transmissions to measure the intensity and phase profiles displayed in Figs. 10-17. In the EM case intensity observations of known tunnels have been done using a CW type technique (Lytle, et al., 1976 & 1977). The results of this work showed profiles comparable to those given above, but with significant amounts of clutter or ambient noise present. Borehole to borehole seismic measurements were made by Cratchley, et al., (1976) to find underground regions of fractured rock. In this case velocity measurements were actually made, but these data could of course be interpreted in terms of phase which we have discussed above. Thus the practicality of borehole to borehole EM and P-wave measurements has been demonstrated by either CW or pulse technique. Lytle, et al., (1976 and 1977) have in fact applied CW measurements to tunnel detection by observing intensity signatures similar to that of Fig. 17. Results include both successful detections and false alarms (Systems Planning Corp., 1979).

E. Signal Analysis

The tunnel detection problem discussed here is the familiar one of detecting a desired signal embedded in a noise background, due in the present case to clutter from unwanted signal propagation paths, to ambient seismic or EM noise and to system noise in the measurement transducers and electronics. There are two distinct problems here: detection of the existence of a tunnel and a description of the tunnel once detected.

1. Detection Methods

a. Matched Filters

The data with which we must make our detection decision (the presence or absence of a tunnel) are the amplitude $A(y)$ and phase $\phi(y)$ of the received electromagnetic or seismic (or other) signal as a function of vertical distance along the sensor borehole y_r (for convenience we will henceforth drop the subscript). In analogy with the more familiar time and frequency domains we consider a spatial distribution domain with coordinate y and the corresponding spatial frequency domain with coordinate s where a function $A(y)$ is moved into the s domain by a Fourier transform which we denote by

$$FT|A(y)| = A'(s) = \int_{-\infty}^{\infty} A(y) \exp(-j2\pi sy)dy \quad .$$

The detection scheme illustrated below would involve chopping the observed signal $A(y)$ or $\phi(y)$ into segments (possibly overlapping), transforming each segment to obtain $A'(s)$ or $\phi'(s)$, applying a filter $H(s)$ to

each A' or ϕ' and observing the filter output for each A' or ϕ'. A statistically significant peak in the filter output would indicate the detection of a tunnel as well as other information we will discuss later.

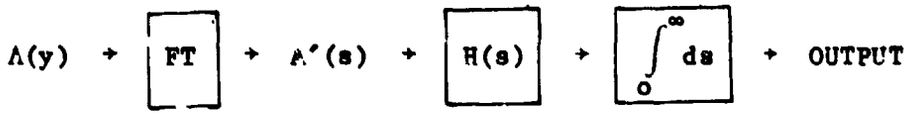

The trick here is to select the filter $H(s)$ in a special way based on a priori knowledge. That is, we determine $H(s)$ based on an expected tunnel signature. Since the tunnel signature changes with such more or less unknown parameters as EM or P-wave speed and tunnel location and diameter, we would probably need to run the data for a succession of "matched filters," $H(s)$ representing a variety of values of these tunnel parameters. Measurements of the propagating medium and other sources of information could narrow the range of parameters to be searched.

By applying a matched filter in the spatial frequency domain one can achieve the optimum detectability of an expected tunnel signature $A_t(y)$ in the sense that the filter output maximizes the peak signature signal to mean noise power ratio (Turin, 1960). The spatial frequency response of the matched filter is given by

$$H(s) = FT[A_t(y)] \exp(-j2\pi s y_1)$$

where y_1 is a fixed reference displacement, e.g., the value of y at the beginning of the sample block used to calculate $A'(s)$. Examination of $H(s)$ reveals that the amplitude spatial spectrum of the matched filter is the same as that of the expected tunnel signature, i.e., $|H(s)| = |A'_t(s)|$. The phase spectrum of the matched filter is the negative of the phase spectrum of the expected tunnel signature plus a phase shift proportional to spatial frequency. The impulse response of the matched filter $h(y)$ is the same as tunnel signature $A_t(y)$ run backwards beginning at y_1, i.e., $h(y) = A_t(y_1 - y)$.

While the matched filter may not be the best way to implement a tunnel detection scheme operationally it provides us with an interesting way to determine how close together measurements should be made along the sensor borehole. Since the matched filter $H(s)$ has some upper frequency cutoff s_c above which $|H(s)|$ is small we need only make measurements sufficient to define $A'(s)$ below s_c. Using the sampling theorem (e.g., see Schwartz and Shaw, 1975) we find that we should make measurements along y at intervals Δy where $\Delta y \leq 1/2s_c$.

b. Correlation Detection

An alternative (and equivalent) way of doing matched filter detection is to make a cross-correlation between the observed signal distributions $A(y)$ or $\phi(y)$ and the expected tunnel signature $A_t(y)$ or $\phi_t(y)$. The expected tunnel signatures are of course also functions of tunnel and propagating medium parameters (location relative to boreholes, size, relative dielectric constant, seismic wave speed, etc.). In this

detect n scheme one simply formulates the cross-correlation function

$$C(y_1) = \int_a^b A_t(y)\ A(y - y_1)\ dy$$

where y_1 is the location of some specific characteristic point in the expected tunnel signature. Detection then involves computing $C(y_1)$ for some selection of t nel and propagating medium parameters and comparing $C(y_1)$ with some threshold value selected as a compromise between probability of detection and false alarm rate. This cross-correlation scheme is probably a more practical means of doing tunnel detection operationally.

2. Parameter Estimation

Once a tunnel is detected one would like to obtain as much descriptive information on the tunnel as possible from the amplitude and phase information at hand $A(y)$, $\phi(y)$. One might also drill additional more advantageous boreholes to obtain further observations. Once a borehole actually enters the tunnel further exploration is possible as discussed in the following chapter. Suppose one has a model for the expected tunnel signature which contains parameters describing the tunnel and propagating medium, such as the diffraction model discussed at length above. Then one can use the observations $A(y)$ and $\phi(y)$ together with the model in a systematic way to estimate the model parameters. Brandt (1976) and Matthews and Walker (1965) discuss methods by which parameters in the model are adjusted such that the closest fit to the observational data, A and ϕ , is obtained in a least squares sense.

Fitting of linear functions of measured quantities to observational data by using a least squares criterion is well-known, e.g., linear regression analysis. Although it involves more complicated and iterative calculations, the least squares concept can be applied to non-linear functions which involve variables not directly observed. This is the case we have here. In this case the observed quantities A and ϕ are expressed as Taylor expansions in the parameters one wishes to estimate, tunnel location, size, etc. The Taylor expansion is initially around a set of "best guesses" for the parameters and an iterative procedure converges by progressing through a sequence of better and better estimates for the desired parameters. Detailed procedures including FORTRAN codes are given by Brandt (1976, Ch. 9).

F. Observational Methods

1. Borehole Scanning

In obtaining the distribution of amplitude and phase along the sensor borehole, $A(y)$ and $\phi(y)$. one is faced with the problem of wanting many sources and sensors so as to obtain much data quickly, but also having to expend the material and manpower resources necessary to obtain them. So, what advantages are there to having more observational data? The basic determining factor in this problem is signal to noise (or clutter) ratio (S/N), i.e., how well the tunnel signature stands out relative to the ambient noise or clutter. As S/N rises, fewer observations are required. While one would not initially know the S/N ratio, information regarding the local geology would be helpful. Also one could begin

with simple observations and progress to more extensive schemes as necessary. Below we discuss increasingly more complex observational schemes. In all cases we assume that the boreholes are drilled so that lines between boreholes are transverse to the long dimension of the expected tunnel, Figs. 7 and 9.

a. Stationary Source with Sensor Scanned

The simplest observational scheme would be to have one source located at the expected tunnel level and one sensor which would traverse along the sensor borehole obtaining $A(y)$ and $\phi(y)$. The diffraction model results of Figs. 10-16 correspond to this case. Multiple sensors along the sensor borehole would speed data collection.

b. Scan with Source and Sensor at Same Level

By moving a single source and sensor combination together (such that $y_r = y_t$ in Fig. 9) one obtains observations corresponding to Fig. 17. Such a scheme involves moving two items and the related uncertainties of location along the borehole. The main advantages of the scheme are that attenuation is minimized by keeping the transmission path short, and ease of interpretation, i.e., constant A and ϕ is expected in the absence of a tunnel. This method is the principal one used by Lytle, et al., (1976, 1977). Again strings of multiple sensors would speed data collection.

c. Multiple Source and Sensor Locations

Data could be collected most quickly and comprehensively by deploying multiple sources and sensors. Multiple sensors and/or

sources, if sufficiently closely spaced, allow for beam forming as with phased array antennas. The matched filter detection approach discussed above could be viewed as a special type of beam forming. Beam forming with a string of sources could also be combined with the matched filter/ correlation approach for the sensor array. Because the propagating medium is rather highly absorbing, especially for EM waves, beam forming is limited since the waves emitted from the ends of the beam forming aperture would be very weak if the aperture were too large. Nevertheless beam forming could be useful, especially in the seismic wave case.

One might be concerned that arrays of multiple sensors would be so complicated to use and the data processing requirements so large that the effort would not be worthwhile. Complications in both observational procedures and data processing software do indeed exist. However, existing computational and data storage hardware are quite adequate to the task even for field operation from a 3/4 ton sized vehicle. Also one would need to consider the trade-off between investment in data processing and multiple sensor and investment in more closely spaced boreholes.

2. Tomography Using Multiple Source and Sensor Locations

Tomographic reconstruction is a technique which uses information gathered along many ray paths passing through the area to be sensed. Along each ray path one measures the line integral of some parameter, for example, seismic or EM wave attenuation or phase change. A set of linear equations is then solved to obtain the desired "image" of

what is contained in the region observed. Dines and Lytle (1979) discuss geophysical applications of the technique in general and Lager and Lytle (1977) apply the technique using VHF radio wave attenuation sounding between boreholes in a coal field. To the author's knowledge the tomographic technique has never been successfully applied to tunnel detection.

In our opinion tomography constitutes a systematic way to analyze tunnel detection data and should not be overlooked. Two areas of improvement come to mind. First, EM wave amplitude may not be the optimum quantity to sense, i.e., seismic wave amplitude or phase or EM wave phase sensing could prove to be the basis of a workable tunnel detection scheme. Second, a vector (rather than a scaler) approach should work better since more information is being used. In this type of tomography a vector quantity, e.g., the received seismic wave phasor (amplitude and phase), is analyzed rather than simply a scaler quantity like EM wave amplitude.

3. Use of Multiple Boreholes--Differential Observations

Since in all probability multiple boreholes will have to be drilled, it is interesting to ask how one might use more than two boreholes by filling the extra boreholes with strings of sources or sensors. Suppose we have three boreholes (A, B and C) spaced 25 m apart in a line transverse to the expected tunnel direction (see Fig. 19). By placing one or more sources in the middle borehole (B) and strings of sensors in the outer boreholes (A and C), one could work a differential detection scheme, e.g.,

using the AB path as a reference with which to compare the BC path and vice versa. Consider a propagation medium which is statistically homogeneous in the horizontal direction, but varies in its properties with depth--a typical though not general case for subterranean propagation (see Fig. 2 and Ollier, 1969). In such a medium the differential scheme will help remove vertically stratified variations in the natural environment which might obscure or be mistaken for a tunnel. Under this assumption the differential scheme would also permit the detection of tunnel signatures when the tunnel is nearer the source than the sensor and the resulting signature is more a variation in overall strength than in signature shape (see Fig. 13a).

As shown in Fig. 13, the tunnel signature is more pronounced when the tunnel is nearer the sensor borehole than the source borehole. This then suggests that one should also obtain data in which sensor and source boreholes are interchanged, i.e., source string in borehole A and sensor string in B as well as vice versa. One could also employ a differential scheme comparing the $A(y)$ and $\phi(y)$ data both before and after the interchange. One could obtain such source-sensor interchange observations by employing the three borehole scheme suggested above and simply moving the distribution of sensor in A, source in B, sensor in C sequentially down a line of boreholes.

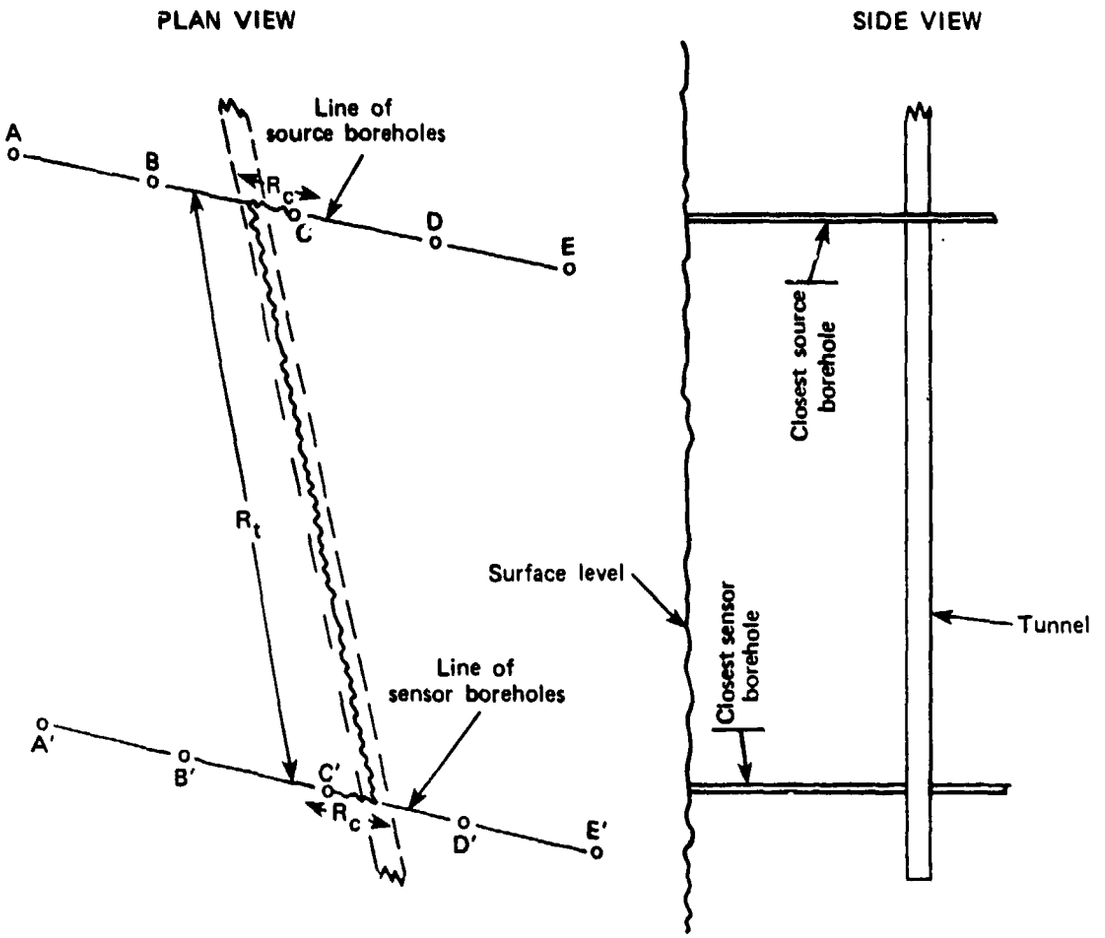

Figure 19. Plan and side views of longitudinal tunnel detection scheme. A line of source boreholes is deployed transverse to the expected tunnel direction and some distance away, but along the expected direction of the tunnel, a string of sensor boreholes is deployed transverse to the expected tunnel direction.

4. Multiple Observations

Let us assume that the inhomogeneities in the subterranean propagation medium can be considered as statistical fluctuations. Under this assumption one could reduce the effect of these fluctuations by averaging. Unfortunately the fluctuations in the propagation change only very slowly with time and hence time domain averaging is not feasible. Some advantage in terms of averaging might be obtained by spatially shifting a string of sensors slightly, e.g., $\mp$ 20% & $\mp$ 40% of the distance between sensors, or changing the operating frequency by $\mp$ 10 or 20%. This would yield sets of observation over which one would average in the hopes of reducing statistical background fluctuations. The idea here is to change the observational frequency or geometry enough to obtain statistically independent samples of the spatial distribution of signal energy scattered by the inhomogeneous propagating medium. Polarization diversity might also be used in this same manner. Figs. 5 and 6 illustrate how the propagating characteristics of geological joints change rapidly with frequency.

IV OTHER TUNNEL DETECTION AND EXPLORATION SCHEMES

The major research effort reported here was directed toward the borehole to borehole EM and seismic wave methods discussed in Chapter III. Several other topics, briefly considered, are discussed below.

A. Borehole to Borehole Sounding Along the Tunnel Direction

In Chapter III we considered borehole to borehole sounding where the boreholes were oriented such that waves travelling between source and sensor would propagate transverse to the tunnel direction. An alternate scheme would take advantage not only of the fact that the tunnel is filled with air rather than rock, but also of the fact that the tunnel provides a long air-filled channel travelling from one place to another. The idea, illustrated in Fig. 19, is to propagate either pulse or continuous wave (CW) signals from source to sensor using the tunnel as a "wave guide" or relatively low-loss propagation medium. Both signal strength and/or phase (or time delay) would be tunnel indicators depending on the different propagation characteristics of the tunnel and the surrounding rock.

1. Propagation Along the Tunnel

While we have not made any extensive investigation of EM or seismic wave propagation along a tunnel, it is clear that a tunnel provides a path which is significantly different from propagation paths in the surrounding rock.

a. Electromagnetic Waves

While tunnels are clearly not designed as wave guides, we note from Wait and Hill (1977):

> "The concept that electromagnetic waves can be guided in tunnel-like structures in the earth is now being exploited for telecommunication purposes by groups in Belgium, France, England, Canada, and the U.S.. The relevant propagation phenomena are much more sophisticated than first envisaged. Some of the complexities are due to the complicated structure of tunnels and haulageways that were designed for ease of transportation rather than communication. Nevertheless, much progress has been made by utilizing idealized models with varying degrees of complexity."

Some further sources of information are Wait (1976 and 1978). Propagation is greatly aided by conductors running along the tunnel. In Fig. 20 we show results obtained by Wait and Hill (1977) for what is known as a surface wave transmission line (SWTL) in a circular tunnel. The SWTL is simply a wire with a dielectric coating. We note that attenuation rate for propagation along the tunnel is a strong function of frequency, thus suggesting that a multiple or swept-frequency system be used and that the frequency range be rather wide. The phase speed of waves along the SWTL is $\sim 0.9c$ at ~ 100 MHz .

b. Seismic Waves

For seismic waves the salient difference between the tunnel and the surrounding medium occurs in terms of compressional wave velocity (~ 330 ms^{-1} in air, but $\sim 2{,}000$ to $5{,}000$ ms^{-1} in rock) rather than in terms of attenuation ($\alpha \sim 0.02$ m^{-1} in either air or rock).

2. Coupling Into and Out of the Tunnel

Given that the tunnel provides an anomalous pathway between source and sensor we must couple energy into the tunnel from the source and out of the tunnel to the sensor. From Fig. 8 and Table III we note that electromagnetic waves are transmitted into the tunnel much more readily than are compressional seismic waves. This occurs because the impedance contrast for seismic waves across an air-rock boundary is orders of magnitude higher than for EM waves across the same boundary. In Fig. 8 we note that the higher impedance contrast implies a higher reflection coefficient at the interface.

3. Detection Methods

Consider the power ratio P_{td} between transmission of EM waves along the tunnel (t) and directly (d) through the subterranean medium. Referring to Fig. 19 we have

$$P_{td} = |E_t|^2/|E_d|^2$$

$$P_{td} = \frac{(4\pi R_c^2)^{-1}\ (4\pi R_c^2)^{-1}\ \exp(-4\alpha_c)\ \exp(-2\alpha_t R_t)}{(4\pi R_t^2)^{-1}\ \exp(-2\alpha_d R_t)}$$

$$P_{td} = [R_c^{-4}\ \exp(-4\alpha_c - 2\alpha_t R_t)]/[4\pi R_t^{-2}\ \exp(-2\alpha_d R_t)]$$

where R_c is the coupling distance between the source (or sensor) and the tunnel and $\exp(-2\alpha_c)$ is the power loss caused by coupling into or out of

the tunnel. Here we have assumed the distances between the tunnel and the source or sensor borehole to be the same, R_c . We also assumed the coupling losses into or out of the tunnel to be equal.

If P_{td} is substantially greater than unity, then the presence of a tunnel should be easily detected by the increase in signal intensity relative to the case where no tunnel is present. As an example, for EM waves let $R_c = 10$ m , $\exp(-2\alpha_c) = 10^{-2}$ (20 dB coupling loss), $\alpha_t = 0.03\ m^{-1}$ (0.3 dB m^{-1} , see Fig. 20), $R_t = 100$ m , $\alpha_d = 0.16\ m^{-1}$ (1.4 dB m^{-1} , see Table 2 for granite at 30 MHz). Substituting in the above formula we have a factor 1.6×10^{-13} loss along the tunnel path compared with a factor 10^{-19} loss along the direct path (no tunnel present). Thus one expects to see an intensity enhancement of $P_{td} \sim 10^6$ when a tunnel is present. It is not so clear what phase shift or time delay effects one can expect. In the case at hand if $\varepsilon_e/\varepsilon_o \sim 5$ in Fig. 19 then one could expect a significantly smaller phase change along the tunnel since $\varepsilon = \varepsilon_o$ in the tunnel. The group delay or time delay for a pulse would presumably be significantly different along the two paths (t and d), but more detailed calculations than attempted here would be required to make a credible estimate of the time delay difference.

So in the EM wave case one would expect to see a sizable increase in intensity when a tunnel is present as well as a change in pulse delay time or phase shift (if CW transmission were used). Differential measurements using boreholes B & B′ as well as C & C′ would make the scheme less subject to variations in the geological setting. Multiple or

swept frequency measurements would be necessary in order to find a frequency range where losses coupling into the tunnel and propagation along the tunnel were reasonably low (see Fig. 20). To obtain the best results one would want to use a frequency range and value of R_t such that a weak, but measureable, signal would propagate between boreholes (e.g., between A & A'). Clearly one would like R_t to be large ($\gtrsim$ 100 m) in order to make P_{td} large. However R_t should not be so large that no signal can be detected in the absence of a tunnel--at HF and VHF radio frequencies a loss of no more than 200 dB (factor 10^{-20}) could be tolerated in practice. To limit the loss while keeping R_t large one would presumably move to lower frequencies where α_d is smaller. Finally one is again faced with the problem of clutter signals propagating along unwanted paths between source and sensor. Hence cables, fences, pipes, etc. running along the expected tunnel direction might have to be removed or at least noted.

In the case of compressional seismic (P) waves the differences between direct propagation and propagation along the tunnel are not nearly so pronounced (as the EM case) in terms of loss, but are pronounced in terms of phase shift or time delay. Since we have seen (in Chapter III) that propagation losses in granite are much smaller for compressional seismic than EM waves at the same frequency, one can operate at larger values of R_t thus exploiting the linear character of the tunnel. However, the coupling loss into and out of a tunnel would be large because of the high impedance contrast (see Fig. 8) thus making the tunnel path losses greater than the direct path.

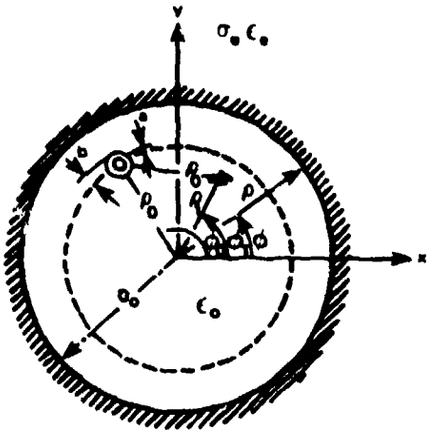

Figure 20a. Cross-section geometry for the SWTL (Surface Wave Transmission Line) located in a circular tunnel and the dipole exciter (after Wait and Hill, 1977).

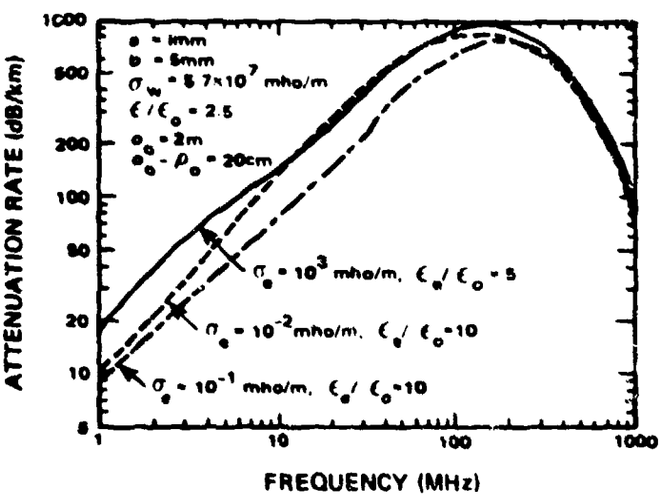

Figure 20b. Influence of the electric properties of the external medium (e.g. Rock) on the attenuation characteristics of the tunnel. σ_w is the conductivity of the wire (after Wait and Hill, 1977).

So for compressional seismic waves one would expect a transmission path with significantly longer time delay to exist when a tunnel is present. However, other shorter time delay paths with approximately the same signal loss would also exist. Hence for a pulse system one would have to detect the presence of a tunnel by looking for a pulse (possibly a weaker one) with an unusually long time delay. This situation is not a good one since one might have to detect the tunnel propagated signal against a background of signals with equally long time delays caused by reflection from the surface, etc. As in the EM wave case a differential scheme using multiple frequencies would prove advantageous.

One could improve this scheme in either the EM or seismic case by the use of strings (arrays) of sources and sensors, thus providing a directable beam in the vertical direction as well as an improvement in signal to noise/clutter because of the array gain. These advantages are at the expense of more sensors, sources and a heavier data processing load. It is conceivable also that this longitudinal propagation scheme might be used with surface seismic sources and sensors.

B. Exploration of a Discovered Tunnel with Electromagnetic and Seismic Waves

Both here and elsewhere great efforts have been expended to detect and localize tunnels with the final confirmation being made by actually drilling a borehole into the tunnel. Once a borehole has actually entered the tunnel it provides an opportunity to introduce EM or seismic

waves directly into the tunnel as well as the current practice of using a borehole camera to look around inside the tunnel.

By transmitting either EM or acoustic pulses down the tunnel and observing echoes (as with a radar or sonar) one could potentially determine the length of the tunnel, obstructions inside it, bends and corners, activity and so forth, since each of these would reflect wave energy back to the receiver. In the case of EM waves one should use a wide range of frequencies as suggested by Fig. 20 where waves at frequencies well below circular waveguide cutoff frequencies can propagate with relatively low attenuation. Since the optimum frequency for probing the tunnel is dependent on unknown factors such as whether or not there are conductors in the tunnel, it would be wise to have a variety of transmission frequencies available and to try them all. In general one would use the highest frequency possible to obtain good spatial resolution, i.e., short pulse length. If continuous wave transmission were used the input impedance of the tunnel could be measured over a variety of frequencies in the hopes of obtaining information about the tunnel by observing resonant frequencies. In a moving target indicator (MTI) mode a "tunnel radar" might be able to detect activity within the tunnel--people or objects moving around.

Acoustic waves could be used to perform the above functions by constructing a "tunnel sonar". Losses for acoustic waves propagating down the tunnel would almost always be a great deal smaller than for EM waves. In addition acoustic plane waves can propagate in the tunnel, thus allowing propagation for wavelengths longer than the cutoff wavelengths for EM

waves. This allows the use of very long wavelengths to observe tunnel resonances which one could presumably interpret in terms of tunnel length, bends, obstructions, etc., as with organ pipes. One disadvantage of acoustic waves is that they can be heard by the human ear, thus alerting people quite obviously that some tunnel observations are in progress. Certainly ultra sound could be used. However one would have to accept greater attenuation ($\lesssim$ 0.1 to 1 m^{-1} amplitude decay at worst) and the difficulty of generating powerful sound waves at these frequencies from inside a borehole. Sound wave attenuation in air is a function of humidity, peaking at $\sim$ 30% relative humidity. So tunnels, being generally damp, would have relatively lower attenuation.

In the scheme described in section A of this chapter a wave was coupled into the tunnel from a nearby borehole source, propagated down the tunnel, and finally detected on a borehole sensor near the tunnel. Clearly being able to have the source directly in the tunnel would be a great aid in this scheme with a successful detection at the sensor and indicating tunnel direction. Such directional information would be quite valuable in determining where to dig an intercept tunnel, particularly if the intercept had to be some distance from the original discovery.

(THIS PAGE LEFT BLANK INTENTIONALLY)

ACKNOWLEDGEMENTS

The authors are happy to acknowledge the willing help of Ernest Blase (formerly of DARPA-TTO), Robert Bohlen and Lambert Dolphin (SRI International), John Fett (consulting geologist) and Ernest Tillotson (British Association for the Advancement of Science) on various technical matters. We thank Joie Borriseau, Jan Fanning, Don LeVine, Elaine Matthews and Kathy Zacher of SRI International for much help in preparation of the manuscript.

(THIS PAGE LEFT BLANK INTENTIONALLY)

REFERENCES

1. D.E. Barrick, "A Note on Scattering from Dielectric Bodies by the Modified Geometrical Optics Method," IEEE Trans. Antennas & Propagat., AP-16, pp. 275-277 (1968).

2. Bowman, G.T., Barrick, D.E., Stuart, W.D. and C.K. Krichbaum (G.T. Ruck, ed.), Radar Cross Section Handbook (2 vols.), Plenum Press, New York (1970).

3. S. Brandt, Statistical and Computational Methods in Data Analysis (2nd ed.), North-Holland, Amsterdam (1976).

4. J.E. Burke, "Low-Frequency Approximations for Scattering by Penetrable Elliptic Cylinders," J. Acoust. Soc. Am., 36, pp. 2059-2070 (1964).

5. Bussey, H.E. and J.H. Richmond, "Scattering by a Lossy Dielectric Circular Cylindrical Multilayer, Numerical Values," IEEE Trans. Antennas & Propagat., AP-23, pp. 723-725 (1975).

6. J.C. Cook, "Radar Transparencies of Mine and Tunnel Rocks," Geophysics, 40, 5, pp. 865-885 (1975a).

7. J.C. Cook, "Status of Ground Probing Radar and Some Recent Experience," Proceedings of Engineering Foundation Conference on "Subsurface Exploration for Underground Excavation and Heavy Construction" (held at Henniker, N.H., Aug. 1974), American Society of Civil Engineers (1975b).

8. Cratchley, C.R., McCann, D.M. and M. Ates, "Application of Geophysical Techniques to the Location of Weak Tunneling Ground, with an Example from the Foyers Hydroelectric Scheme, Loch Ness," Trans. Inst. Min Met., 85, pp. A127-A135 (1976).

9. Dines, K. A. and R. J. Lytle, "Computerized Geophysical Tomography," Proc. IEEE, 67, 1065-1073 (1979).

10. Gates, D.C. and R.A. Armistead, "The Use of Advanced Technologies for Locating Underground Obstacles," Final Report EPRI 78-20-0, Electric Power Research Institute, 3412 Hillview Ave., Palo Alto, CA 94304 (1974).

11. J.W. Goodman, Introduction to Fourier Optics, McGraw-Hill, San Francisco (1968).

12. W.K. Hamblin, Earth's Dynamic Systems, Burgess, Minneapolis, Minnesota (1975).

13. R.F. Harrington, Field Computation by Moment Methods, Roger F. Harrington, R.D.2, West Lake Rd., Cazenovia, N.Y. 13035 (1968).

14. S.J. Hoon, The Korean Tunnels--Where They Really Lead, Far Eastern Review article reported in San Francisco Chronicle, p. 7, 11 November 1978.

15. Jenkins, F.A. and H.E. White, Fundamentals of Optics, McGraw-Hill, New York (1976).

16. Keller, G.V. and F.C. Frischknecht, Electrical Methods in Geophysical Prospecting, Pergamon Press, New York, N.Y. (1960).

17. King, R.W.P. and T.T. Wu, The Scattering and Diffraction of Waves, Harvard Univ. Press, Cambridge, Mass. (1959).

18. Kouyoumjian, R.G., Peters, L. and D.T. Thomas, "A Modified Geometrical Optics Method for Scattering by Dielectric Bodies," IEEE Trans. Antennas & Propagat., AP-11, pp. 690-703 (1963).

19. Kraichman, M.B., Handbook of Electromagnetic Propagation in Conducting Media, U.S. Govt. Printing Office, Washington, D.C. 20402 (1970).

20. Lager, D. L. and R. J. Lytle, "Determining a Subsurface Electromagnetic Profile from HF Measurements by Applying Reconstruction Technique Algorithms," Radio Sci., 12, 249-260 (1977).

21. R.J. Lytle, "Far Field Patterns of Point Sources Operated in the Presence of Dielectric Circular Cylinders," IEEE Trans. Antennas Propagat., AP-19, pp. 618-621 (1971).

22. Lytle, R.J. and D.L. Lager, "The Yosemite Experiments: HF Propagation Through Rock," Radio Sci., 11, pp. 245-252 (1976).

23. Lytle, R.J. Lager, D.L., Laine, E.F. and D.T. Davis, "Finding a Tunnel Using Cross-Borehole Electromagnetic Probing" (U) in Working Papers on Tunnel Detection from the Meeting of 11 November 1976, Stanford Research Inst., Menlo Park, CA 94025 (1976) CONFIDENTIAL (The paper by Lytle, et al., is UNCLASSIFIED).

24. Lytle, R.J., Lager, D.L., Laine, E.F. and D.T. Davis, "Finding High-Contrast Anomalies Using Radio Waves" in Working Papers on Tunnel Detection from the Meeting of 7 April 1977, Vol. I, Stanford Research Inst., Menlo Park, CA 94025 (1977).

25. Matthews, J. and R.L. Walker, Mathematical Methods of Physics, Benjamin, N.Y. (1965).

26. Microwave Asso. Inc., "Terrascan," Bulletin 8002, Microwave Asso. Inc., Burlington, MA (1976).

27. B.J. Morse, "Diffraction by Polygonal Cylinders," J. Math. Phys., 5, pp. 199-215 (1964).

28. C. Ollier, Weathering, American Elsevier, New York (1969).

29. Officer, C. B., Introduction to Theoretical Geophysics, Springer-Verlag, N.Y., (1974).

30. D.S. Parasnis, Principles of Applied Geophysics, Chapman & Hall, London (1972).

31. E.I. Parkhomenko, Electrical Properties of Rocks, Plenum Press, New York, N.Y. (1967).

32. Pearce, D.C., Hulse, W.H. & J.W. Walker, "The Application of the Theory of Heterogeneous Dielectrics to Low Surface Area Soil Systems," IEEE Translations on Geoscience Electronics, GE-11, 4, pp. 167-170 (1973).

33. Peters, L., "Video Pulse Radar" in Stanford Research Institute (1976a).

34. Ramo, S., Whinnery, J.R. and T. Van Duzer, Fields and Waves in Communications Electronics, Wiley, New York (1965).

35. Ruck, G.T., Banick, D.E., Stuart, W.D. and C.K. Krichbaum (G.T. Ruck, ed.), Radar Cross Section Handbook (2 vols.), Plenum Press, New York (1970).

36. Schwartz, M. and L. Shaw, Signal Processing, McGraw-Hill, N.Y. (1975).

37. S. Silver, "Microwave Aperture Antennas and Diffraction Theory," J. Opt. Soc. Am. 52, p. 131 (1962).

38. A.Sommerfeld, Optics, Vol. IV of Lectures on Theoretical Physics, Academic Press, New York (1964).

39. Stanford Research Inst., Working Papers on Tunnel Detection from the Meeting of 11 November 1976, Contract DAAG 53-76-C-0177, Stanford Research Inst., Menlo Park, CA 94025 (1976b) CONFIDENTIAL (Much of the document is UNCLASSIFIED material.)

40. Stanford Research Inst., Working Papers on Tunnel Detection from the Meeting of 7 April 1977, Vol. I, Contract DAAG 53-76-C-0177, Stanford Research Inst., Menlo Park, CA 94025 (1977).

41. Stanford Research Inst., Working Papers on Tunnel Detection from the Meeting of 3 June 1976, Contract DAAG 53-76-C-0177, Stanford Research Inst., Menlo Park, CA 94025 (1976a) CONFIDENTIAL (Much of the document is UNCLASSIFIED material.)

42. Systems Planning Corporation, A Summary of the DARPA Program of Tunnel Detection Technology (compiled under subcontract by Robert Bollen and Lambert Dolphin of SRI International), SPC Rpt. #459, Systems Planning Corporation, 1500 Wilson Blvd., Rosslyn, VA (June 1979) CONFIDENTIAL.

43. Telford, W.M., Geldart, L.P., Sheriff, R.E. and D.A. Keys, Applied Geophysics, Cambridge University Press, Cambridge (1976).

44. G.N. Tsandoulas, "Scattering of a Dipole Field by Finitely Conducting & Dielectric Circular Cylinders," IEEE Trans. Antennas & Propagat., AP-16, pp. 324-328 (1968).

45. G.L. Turin, "An Introduction to Matched Filters," IRE Trans., IT-6, pp. 311-329 (1960). This number was a special issue on matched filters.

46. R.S. Vickers, "Remote Sensing of Soil Mantle," Final Report SRI Project 4656, Stanford Research Inst., Menlo Park, CA 94025 (1976).

47. Verhoogen, J., Turner, F.J., Weiss, L.E., Wahrhaftig, C. and W.S. Fyfe, The Earth, an Introduction to Physical Geology, Holt, Rinehart and Winston, New York (1970).

48. J.R. Wait, "The Effect of a Buried Conductor on the Sub-Surface Fields for Line Source Excitation, Radio Sci, 7, pp. 587-591 (1972).

49. Wait, J.R. and D.A. Hill, "Electromagnetic Fields of a Dipole Source in a Circular Tunnel Containing a Surface Wave Line," Int. J. Electronics, 42, pp. 377-391 (1977).

50. J.R. Wait (ed.), Electromagnetic Probing in Geophysics, Golem Press, Boulder, Colo. (1971).

51. J.R. Wait (ed.), "Electromagnetic Waves in Mine Environments, Cooperative Institute for Research in Environmental Sciences," University of Colorado/N.O.A.A., Boulder, Colorado 80309 (1978).

52. Wait, J.R. and D.A. Hill, "Electromagnetic Fields of a Dipole Source in a Circular Tunnel Containing a Surface Wave Line," Int. J. Electronics, 42, pp. 377-391 (1977).

53. J.R. Wait (ed.), "Subsurface Telecommunications and Geophysical Probing," Special Issue, Radio Science, 11, pp. 233-418 (1976).

54. Watt, A.D., Mathews, F.S. and E.L. Maxwell, "Some Electrical Characteristics of the Earth's Crust," Proc. IEEE, ?, pp. 897-910 (1963).

55. T.G. Winter, "A Survey of Sound Propagation in Soils," in Acoustical Holography, Vol. 5, (P.S. Green, ed.), Plenum Press, New York, N.Y. (1974).

56. J.E. White, Seismic Waves, McGraw-Hill, New York (1965).

(THIS PAGE LEFT BLANK INTENTIONALLY)

DISTRIBUTION LIST

ORGANIZATION	NO. OF COPIES
Dr. Arden Bement Deputy Under Secretary of Defense for R&AT Room 3E114, The Pentagon Washington, D.C. 20301	2
Mr. Robert L. Bollen SRI International 333 Ravenswood Avenue Menlo Park, CA 94025	1
Mr. Wayne Boring P.O. Box 1925 Washington, D.C. 20013	1
Dr. Gregory Canavan Director, Office of Inertial Fusion, U.S. DOE M.S. C404 Washington, D.C. 20545	1
Dr. Robert Clark P.O. Box 1925 Washington, D.C. 20013	1
Cmdr. Robert Cronin NFOIO Detachment, Suitland 4301 Suitland Road Washington, D.C. 20390	1
Defense Documentation Center Cameron Station Alexandria, VA 22314	12
Dr. Alvin M. Despain 1192 Grizzly Peak Boulevard Berkeley, CA 94708	1
The Honorable Gerald P. Dineen Assistant Secretary of Defense, (C^3I) Room 3E1014, The Pentagon Washington, D.C. 20301	1
Mr. Lambert Dolphin SRI International 333 Ravenswood Avenue Menlo Park, CA 94025	1
Dr. David D. Elliott SRI International 333 Ravenswood Avenue Menlo Park, CA 94025	1
Director National Security Agency Fort Meade, MD 20755 ATTN: Mr. Richard Foss, A42	2
Dr. Robert Fossum, Director DARPA 1400 Wilson Boulevard Arlington, VA 22209	2
Mr. John Fett c/o Lambert Dolphin SRI International 333 Ravenswood Avenue Menlo Park, CA 94025	1
Dr. Edward A. Frieman Director, Office of Energy Research, USDOE M.S. 6E084 Washington, D.C. 20585	1
Dr. George Gamota OUSDRE (R&AT) Room 3D1067, The Pentagon Washington, D.C. 20301	3
Dr. Richard L. Garwin IBM, TJWatson Research Center P.O. Box 218 Yorktown Heights, NY 10598	1
Director National Security Agency Fort Meade, MD 20755 ATTN: Mr. Thomas Handel, A243	1

ORGANIZATION	NO. OF COPIES
Dr. Robert J. Hermann Assistant Secretary of the Air Force (RD&L) Room 4E856, The Pentagon Washington, D.C. 20330	1
Dr. Benjamin Huberman Associate Director, OSTP Room 476, Old Executive Office Building Washington, D.C. 20506	1
Mr. Eugene Kopf Principal Deputy Assistant Secretary of the Air Force (RD&L) Room 4E964, The Pentagon Washington,D.C. 20330	1
Dr. I. L. Lager Lawrence Livermore Laboratory Livermore, CA 94550	1
Mr. Ray Leadabrand SRI International 333 Ravenswood Avenue Menlo Park, CA 94025	1
Mr. Robert Leonard SRI International 333 Ravenswood Avenue Menlo Park, CA 94025	1
Mr. Barry Leven NISC/Code 20 4301 Suitland Road Washington, D.C. 20390	1
Dr. Donald M. LeVine SRI International 1611 N. Kent Street Arlington, VA 22209	3
Dr. R. J. Lytle Lawrence Livermore Laboratory Livermore, CA 94550	1
Director National Security Agency Fort Meade, MD 20755 ATTN: Mr. Robert Madden, R/SA	2

ORGANIZATION	NO. OF COPIES
Mr. John Meson DARPA 1400 Wilson Boulevard Arlington, VA 22209	1
Dr. Julian Nall P.O. Box 1925 Washington, D.C. 20013	1
Prof. William A. Nierenberg Scripps Institution of Oceanography University of California La Jolla, California 92093	1
The Honorable William Perry Under Secretary of Defense (R&E) Office of the Secretary of Defense Room 3E1006, The Pentagon Washington, D.C. 20301	1
Dr. Leon Peters Electrical Engineering Dept. Ohio State University Columbus, OH	1
Dr. Art Shef P.O. Box 1925 Washington, D.C. 20013	1
SRI/MP Reports Area G037 333 Ravenswood Avenue Menlo Park, CA 94025 ATTN: D. Leitner	3
Dr. John F. Vesecky Center for Radar Astronomy Stanford University Stanford, CA 94305	10
Mr. R. S. Vickers SRI International 333 Ravenswood Avenue Menlo Park, CA 94025	1